Structural and Biochemical Analysis of the *Hordeum vulgare* L. *Hv*GR-RBP1 Protein, a Glycine-Rich RNA-Binding Protein Involved in the Regulation of Barley Plant Development and Stress Response

Brian P. Tripet,[‡] Katelyn E. Mason,[‡] Brian J. Eilers,[‡] Jennifer Burns,[‡] Paul Powell,[‡] Andreas M. Fischer,[§] and Valérie Copié*,[‡]

[‡]Department of Chemistry and Biochemistry and [§]Department of Plant Sciences and Plant Pathology, Montana State University, Bozeman, Montana 59717, United States

S Supporting Information

ABSTRACT: The timing of whole-plant senescence influences important agricultural traits such as yield and grain protein content. Post-transcriptional regulation by plant RNA-binding proteins is essential for proper control of gene expression, development, and stress responses. Here, we report the three-dimensional solution NMR structure and nucleic acid-binding properties of the barley glycine-rich RNA-binding protein *Hv*GR-RBP1, whose transcript has been identified as being >45-fold up-regulated in early—as compared to late—senescing near-isogenic barley germplasm. NMR analysis reveals that *Hv*GR-RBP1 is a multidomain protein comprising a well-folded N-terminal RNA Recognition Motif (RRM) and a structurally disordered C-terminal glycine-rich domain. Chemical shift differences observed in 2D ^{1}H$-^{15}$N correlation (HSQC) NMR spectra of full-length *Hv*GR-RBP1 and N-*Hv*GR-RBP1 (RRM domain only) suggest that the two domains can interact both in-trans and intramolecularly, similar to what is observed in the tobacco *Nt*GR-RBP1 protein. Further, we show that the RRM domain of *Hv*GR-RBP1 binds single-stranded DNA nucleotide fragments containing the consensus nucleotide sequence 5′-TTCTGX-3′ with low micromolar affinity *in vitro*. We also demonstrate that the C-terminal glycine-rich (*Hv*GR) domain of *Hv*-GR-RBP1 can interact nonspecifically with ssRNA *in vitro*. Structural similarities with other plant glycine-rich RNA-binding proteins suggest that *Hv*GR-RBP1 may be multifunctional. Based on gene expression analysis following cold stress in barley and *E. coli* growth studies following cold shock treatment, we conclude that *Hv*GR-RBP1 functions in a manner similar to cold-shock proteins and harbors RNA chaperone activity. *Hv*GR-RBP1 is therefore not only involved in the regulation of barley development including senescence, but also functions in plant responses to environmental stress.

Senescence is the final stage in a monocarpic plant's life cycle and is critical for plant reproduction, crop yield, and the grain protein content of its seeds. This highly coordinated and active molecular process involves the dismantling of leaf cellular components, degradation of cell constituents, and remobilization of nutrients, in particular, nitrogen, to developing seeds in annual plants, or stems and roots in perennial species.[1,2]

The timing of whole-plant and leaf senescence is genetically controlled. However, senescence can also be induced by a variety of environmental factors such as light intensity and duration, temperature, nutrient availability, pathogens, and other environmental stresses, indicating that cross-talk exists between biochemical signaling pathways modulating abiotic and biotic stress responses and those controlling developmentally regulated plant senescence. Despite the biochemical complexity of plant senescence, significant advances have been made in our understanding of critical components of signaling pathways that regulate leaf senescence. This knowledge has arisen by characterizing biochemical traits of plant lines and varieties varying in their senescence behavior and the function of senescence-associated genes. Despite these

advances, it is clear, however, that more complete molecular characterizations of specific regulatory factors associated with the process of plant senescence are needed.

Hordeum vulgare L. (barley) is one of the most economically important cereal crops grown worldwide. Barley seeds are used for food, as a principal feed for livestock, or for malting for alcoholic beverage production.[3] The timing of senescence strongly impacts barley yield and the grain protein content (GPC) of its seeds. Early senescing barley plants generate seeds that are high in GPC and more ideally suitable as feed, whereas late-senescing barley plants produce seeds with a lower GPC and higher carbohydrate content,[2,4] characteristics that are preferred for malting.[3] The characterization of senescence-associated gene products in cereals such as barley is critical to help us understand how senescence signaling pathways modulate GPC and affect crop yield and crop quality. Ultimately, data generated by fundamental biochemical studies

of molecular processes critical to barley senescence will be useful to develop new barley varieties that have been modified with respect to senescence initiation and timing for optimal and specific agro-economic purposes.

Previously, RNA transcripts extracted from the topmost leaves (i.e., leaves growing directly below the barley ears) of a late-senescing barley variety, referred to as "Karl", were compared to those of a near-isogenic early senescing barley line, referred to as "10_11", at 14 and 21 days past anthesis (dpa) (i.e., past flowering). The two barley varieties "Karl" and "10_11" vary genetically in the allelic state of a particular locus on chromosome 6H, which was shown to influence leaf senescence and grain protein content of these two barley lines.[5−7] As anticipated, the earlier senescing "10_11" barley line displayed increased abundance of gene transcripts related to Senescence Associated Genes (SAGs) which code for proteins with putative or established roles in senescence, such as transcription factors, kinases, phosphatases, lipases, pro-teases, and nucleases. Interestingly, a transcript coding for a putative RNA-binding protein termed HvGR-RBP1 (GenBank JX126694) was identified as one of the most up-regulated gene transcripts (i.e., >45-fold) in the early senescing "10_11" barley line, when compared to its transcript level in the late senescing "Karl" variety.[5]

Examination of its amino acid sequence indicated that HvGR-RBP1 shares 65% protein sequence identity with the Arabidopsis thaliana RNA-binding protein AtGRP7 which has been implicated in the regulation of flowering, and has been shown to be up-regulated during Arabidopsis senescence.[8,9] Specifically, Atgrp7 T-DNA mutant and RNAi interference Arabidopsis lines with reduced levels of AtGRP7 flowered late when compared to wild-type plants under both long- and short-day conditions, but this late-flowering phenotype was canceled by vernalization.[8] Similarly, the late-senescing barley variety "Karl" with very low Hvgr-rbp1 expression flowered later than "10_11" (with high Hvgr-rbp1), and as in Arabidopsis, these differences disappeared when plants were vernalized.[10,11] These observations thus suggest that strong functional similarities exist between HvGR-RBP1 and AtGRP7.

Further inspection of the amino acid sequence of HvGR-RBP1 suggests that the protein is composed of a highly conserved N-terminal RNA Recognition Motif (RRM) spanning residues 1−92, and a C-terminal glycine-rich region containing a series of (GGR or RGG) amino acid repeats, spanning residues 93−162 of full-length HvGR-RBP1. This protein thus appears to be a member of a large family of less well-characterized plant glycine-rich RNA-binding proteins (referred to as GR-RBPs), which are implicated in the regulation of diverse cellular processes including plant develop-ment, responses to environmental stress, and post-transcrip-tional gene regulation.[12−19]

While the structural architectures of several eukaryotic RRM-containing proteins have been reported,[20−22] our structural and functional understanding of plant RRM and plant glycine-rich RNA-binding proteins is less well developed. To this date, the three-dimensional (3D) structures of only two plant-derived GR-RBPs have been reported,[23,24] and none from barley. The present work is the first structural report of a barley GR-RBP protein.

In this work, we report structural and biochemical findings regarding barley HvGR-RBP1, including a detailed character-ization of the 3D structure of its N-terminal RRM domain, and the nucleic acid binding properties of full-length HvGR-RBP1

and of its associated RRM and glycine-rich (GR) domains. Our structural studies indicate that HvGR-RBP1 is a bipartite protein, comprised of a well-folded RNA Recognition Motif (RRM) at its N-terminus, and a largely unstructured glycine-rich (GR) C-terminal domain.

Moreover, protein−protein interactions were detected using NMR chemical shift perturbation experiments between the RRM and GR domains of HvGR-RBP1, suggesting that at least in vitro, these two domains self-associate, results that are consistent with what has been observed for the Nicotiana tabacum NtGR-RBP1 protein.[24] Nucleic acid interaction assays indicated that the GR domain of HvGR-RBP1 can bind to single-stranded RNA (ssRNA) in the absence of the RRM domain. As anticipated based on the HvGR-RBP1 sequence similarity to the Nicotiana tabacum NtGR-RBP1 protein and a recent report by Khan et al.,[24] ^{1}H/^{15}N chemical shift perturbation experiments established that the N-terminal RRM domain of HvGR-RBP1 can bind, albeit weakly, to a 6-nucleotide single-stranded DNA fragment containing the consensus sequence 5′-TTCTGX-3′, a DNA equivalent of the 5′-UUCUGA-3′ RNA sequence previously identified as a key nucleotide binding motif for the Arabidopsis protein AtGRP7.[25] Taken together, these results suggest a model of nucleotide binding for HvGR-RBP1 involving cooperative binding of single-stranded nucleic acid targets and the RRM and GR domains of HvGR-RBP1. In addition, our observations that expression levels of the barley Hvgr-rbp1 transcript are increased under cold stress, and that the protein enhances E. coli growth following cold-shock treatment, strongly suggest that HvGR-RBP1 harbors RNA chaperone activity in addition to its ability to bind single-stranded nucleic acids.

■ MATERIALS AND METHODS

Cloning, Protein Expression, and Purification. Plasmid constructs encoding amino acid residues 1−162 (FL-HvGR-RBP1), 1−137 (137-HvGR-RBP1), 1−112 (112-HvGR-RBP1), 93−162 (HvGR), and 1−92 (N-HvGR-RBP1) of HvGR-RBP1 were prepared similarly to that described in ref 26. The vector encoding the FL-HvGR-RBP1(F54A) protein variant was generated using the QuikChange Lightening (Agilent Tech-nologies) site directed mutagenesis kit using pET46-FL-HvGR-RBP1 vector as the starting template. For pET32-C-HvGR-RBP1, DNA coding for amino acid residues 93−162 of HvGR-RBP1 was amplified using PCR from pET46-FL-HvGR-RBP1 and ligated into pET-32 Xa/LIC (Novagen) plasmid. The proteins expressed using the pET46 expression vectors resulted in protein constructs containing a 6-histidine tag for purification and added the following 14 residues MAHH-HHHHVDDDDK to the native sequences, as previously reported.[26]

Recombinant protein expression was carried out using Escherichia coli BL21(DE3) (Invitrogen) cells transformed with plasmids containing Hvgr-rbp1 constructs and grown at 37 °C in LB supplemented with 50 μg/mL ampicillin for 6 h, followed by induction of protein synthesis via addition of 1 mM isopropyl-β-D-thiogalactoside (IPTG) to cell cultures at an OD$_{600}$ of 0.6. For production of uniformly ^{15}N or ^{15}N/^{13}C labeled HvGR-RBP1 proteins, transformed BL21 cells were grown in M9 minimal media containing ^{15}NH$_4$Cl (1 g/L) and [^{13}C$_6$]-glucose (2g/L) (Cambridge Isotope Lab) as the sole sources of nitrogen and carbon, respectively. Following 10 h of cell growth post IPTG induction, bacterial cells were harvested by centrifugation, resuspended in 250 mM NaH$_2$PO$_4$, 1 M

NaCl, 10 mM imidazole, 0.1 mM PMSF, pH 8 buffer, and lysed using an M-110L microfluidizer (Microfluidics). Cell debris were subsequently removed by centrifugation at 24 000g for 20 min, and resulting supernatant applied to a nickel affinity column containing 3−5 mL bed volume of HisPur-Ni-NTA resin (ThermoScientific), followed by protein elution using standard nickel affinity column wash and purification procedures.[26] Protein-containing fractions were pooled and dialyzed twice against 1 L buffer solution containing 50 mM NaH$_2$PO$_4$/Na$_2$HPO$_4$, 300 mM NaCl, 0.1 PMSF, at pH 6.8, and resulting HvGR-RBP1 protein was further purified by gel filtration using a Superdex 75 size exclusion column (1 × 30 cm, GE Life Sciences) pre-equilibrated in the same buffer. Final protein containing fractions were pooled and concentrated to 1 mM protein concentration as determined by Bradford (Bio-Rad) assay and OD$_{280}$ nm absorbance readings. Similar purification protocols were used for all HvGR-RBP1 protein constructs of interest. For NMR analysis of ^{15}N-labeled FL-HvGR-RBP1 which displayed significant aggregation properties at 1 mM, 2D ^{1}H−^{15}N correlation (HSQC) NMR experiments were also performed on samples at different pH conditions (pH 6.2, 6.8, and 7.2), temperature (298 and 303 K), and more dilute sample concentrations (0.25 mM). Resulting spectra for FL-HvGR-RBP1 were compared to the 2D ^{1}H−^{15}N correlation NMR spectra acquired for ^{15}N-labeled N-HvGR-RBP1 under the same conditions.

NMR Spectroscopy. Multidimensional NMR spectra of N-HvGR-RBP1 were acquired at 298 K (25 °C) in 50 mM NaH$_2$PO$_4$/NaH$_2$PO$_4$, 300 mM NaCl, 1 mM EDTA, 0.1 mM PMSF, 0.01% NaN$_3$ pH 6.8, containing 10% (v/v) D$_2$O or 100% D$_2$O (for acquisition of 3D ^{13}C-edited ^{1}H−^{1}H-TOCSY, ^{1}H−^{1}H-NOESY, and 2D ^{1}H−^{13}C-CT-HSQC spectra) buffer using a 5 mm triple axis (^{1}H, ^{15}N, ^{13}C) TCI cryogenically cooled probe (cryoprobe) and a Bruker AVANCE III 600-MHz (^{1}H Larmor frequency) NMR spectrometer. NMR spectra were processed using NMRPipe[27] and analyzed using the software program Sparky.[28] Chemical shift assignments of backbone and side-chain atoms (^{1}H, ^{13}C, ^{15}N) were obtained using the following double and triple resonance solution NMR experiments: ^{1}H−^{15}N-HSQC, ^{1}H−^{13}C-CT-HSQC, HNCA, HNCACB, CBCA(CO)NH, CC(CO)NH, HBHA(CO)NH, H(CCCO)NH, HCCH-TOCSY, (HB)CB(CGCDCE)HE, and (HB)CB(CGCD)HD, as reported in ref 26. ^{1}H, ^{13}C, and ^{15}N chemical shifts were indirectly referenced to DSS. Dihedral angle (ϕ and ψ) restraints were obtained from chemical shift data using the program TALOS+.[29] Interproton distance restraints were obtained from 3D ^{15}N-edited and ^{13}C-edited NOESY spectra using a combination of automated and manual assignment methods. Hydrogen-bond restraints were determined using the algorithm VADAR[30] in combination with H$_2$O/D$_2$O solvent exchange experiments that were performed by first lyophilizing 500 μL of a 1 mM ^{15}N-labeled N-HvGR-RBP1 protein sample, followed by resuspension of the lyophilized protein in the same volume of 100% D$_2$O, and acquisition of a series of 2D ^{1}H−^{15}N-HSQC correlation spectra at subsequent time points. Additionally, a 2D-CLEANEX-PM NMR experiment[31] was performed to detect amide protons participating in fast chemical exchange with solvent.

NMR Structure Calculations. 3D structure determination of N-HvGR-RBP1 was achieved using standard simulated annealing protocols as implemented in the program CYANA,[32,33] and NMR chemical shifts, dihedral angles, and NOE-derived interproton distance restraints as experimental

input constraints. From a set of 200 structures generated, 40 conformers with the lowest residual target function values were selected and subjected to further restraints minimization with AMBER9[34] using the AMBER 2003 force field, a generalized Born model, and a 10 Å TIP3P water box of the AMPS-NMR web portal.[35] From these calculations, the 20 lowest conformational energy conformers most consistent with the experimental NMR data were chosen as representative conformers of the ensemble of N-HvGR-RBP1 protein structures. The stereochemistry and quality of these structures were analyzed using PROCHECK-NMR,[36] MolProbity,[37] Verify3D,[38] and the protein structure validation suite (PSVS) software.[39] Statistics resulting from the structural calculations and assessment of the structural quality of the calculated protein models are presented in Table 1. An ensemble of the 20 lowest energy conformers of

Table 1. Structural Statistics for the Ensemble of N-HvGR-RBP1 NMR Structures

Constraints for final structure calculations	
Total NOE distance restraints	683
Intraresidue	352
Sequential ($|i − j| = 1$)	165
Medium range ($1 < |i − j| < 5$)	46
Long range ($|i − j| \geq 5$)	120
Dihedral angle restraints[a]	
Φ angles	83
Ψ angles	83
Hydrogen bond distance restraints[b]	74
Structure statistics (20 conformers)	
CYANA target function (Å^2)	0.58
Residual distance violations	
Number >0.5 Å	0
Number >0.3 Å	0
Residual dihedral angle violations	
Number >5°	0
AMBER mean restraint violation energy (kcal/mol)	6.11
Ramachandran plot statistics (%)[c]	
Residues in most favored regions	85.3
Residues in additionally allowed regions	13.6
Residues in generously allowed regions	1.2
Residues in disallowed regions	0
Average RMSD to mean structure (Å)[d]	
Protein backbone	0.66 ± 0.14
Protein heavy atoms	1.36 ± 0.18

[a]Φ and Ψ angles were derived from the program TALOS+, based on the ^{13}C$^\alpha$, ^{13}C$^\beta$, ^{13}CO, ^{1}H$^\alpha$, and ^{15}N chemical shifts. [b]Two distance restraints between amide and carbonyl group atoms (NH−O = 1.8−2.8 Å, N−O = 2.5−3.8 Å) were used for the hydrogen bond restraints. [c]Ramachandran plot analysis performed using PROCHECK_NMR. [d]Residues 10 through 84 were used in the RMSD calculations.

N-HvGR-RBP1 has been deposited in the Protein Data Bank as PDB entry 2MPU, and BMRB code 18776 for the NMR constraints. Figures were prepared using PYMOL software.[40] Structural homologues were identified using the DALI web server,[41,42] and amino acid sequence homologues were identified using the NCBI BLAST web server[43] and aligned using the Clustal Omega alignment server.[44]

In Vitro **Transcription and Generation of Single Stranded RNA (ssRNA).** Using standard Qiagen cloning methods, the *Hvgr-rbp1* (GenBank id: JX126694) gene was cloned into a pDrive cloning vector and used as template for *in*

vitro transcription and production of single-stranded RNA (ssRNA). More specifically to generate ssRNA, 2.5 μg of plasmid DNA in 20 μL was linearized by restriction digest with Sal1 (*Promega*) for 2 h at 37 °C and heated at 65 °C for 20 min. The resulting sample was treated with 40 units of RNase inhibitor (New England BioLabs), followed by addition of T7 RNA polymerase (50 units plus nucleotide containing buffer) and the reaction incubated for 2 h at 37 °C. To remove the DNA template, the sample was subsequently treated with DNase I (New England Biolabs), and the ssRNA isolated using QIAGEN RNeasy spin columns (Qiagen).

Generation of Single Stranded DNA Templates (ssDNA). DNA coding for *Hv*GR-RBP1 was amplified by PCR using a pET46-FL-*Hv*GR-RBP1 vector as template and biotin-5′-GACGACGACAAGATGGCAGAGTCGGACGGC-GCCG and 5′-GAGGAGAAGCCCGGTTCAGTATCC-GTCGGAGTTGCCTCCGCG primers. The PCR product was purified using the QIAquick gel extraction kit (Qiagen) and eluted in TE (20 mM Tris-HCl, pH 8.0, 150 mM NaCl, 1 mM EDTA) buffer. Streptavidin beads (100 μL) placed in a mini-microcentrifuge filter unit were washed with 2 × 1 mL 20% (v/v) aqueous ethanol and 2 × 1 mL TE buffer. Gel purified DNA (3 μg) was added to the beads in 1 mL TE buffer and slow-tilt rotated for 1 h. The beads were then washed with 2 × 1 mL TE buffer and 2 × 1 mL H₂O, and resuspended in 100 μL of 20 mM NaOH and slow tilt-rotated for 10 min. Following centrifugation, the supernatant was removed and 40 mM HCl added to bring the solution pH back to 7.0. The concentration and purity of the ssDNA was determined by UV spectroscopy and agarose gel electrophoresis.

Gel Electrophoretic Mobility Shift Assay (EMSA). Purified protein samples (FL-*Hv*GR-RBP1, N-*Hv*GR-RBP1; 137-*Hv*GR-RBP1) were dialyzed against nucleic acid binding buffer (25 mM Tris-HCl, 10 mM HEPES, 1 mM EDTA, 50 mM NaCl, pH 7.8) and diluted to 4.4 μM with binding buffer supplemented with 40 units of RNase inhibitor (New England Biolabs) and 50 μg/mL bovine serum albumin. In a 10 μL reaction volume, 1 μL of ssRNA, ssDNA, or dsDNA (stock concentrations of 125 ng/μL, 0.042 μM, 900 bp) was mixed with increasing concentrations of protein (from 0 μM to 1.0 μM) and incubated at 25 °C for 30 min. Loading buffer (2.5 μL of 20 mM Tris-HCl, 10 mM EDTA, 50% glycerol, pH 7.8) was added, and the total sample mixture analyzed on a 1.2% agarose gel with 0.5× TBE running buffer run at 60 V for 45 min, and visualized under UV light following SybrGold (Invitrogen) staining.

Preparation of ssRNA-Bound Affinity Chromatography Columns. Covalent coupling of ssRNA (25 μg) to 200 mg of cyanogen-bromide (CNBr)-activated Sepharose beads was carried out as described in ref 45. Barley plant RNA was isolated from leaf samples (300 mg) and bacterial RNA was isolated from *E. coli* (from 200 mg of wet cell pellet) using standard protocols and the Trireagent (Sigma-Aldrich).

NMR Studies of *Hv*GR-RBP1 Binding to Single Stranded DNA (ssDNA). Interactions between N-*Hv*GR-RBP1 and single stranded DNA nucleotide sequences (5′-TTCTGG-3′, 5′-CTGTTG-3′, 5′-TTCTGA-3′, 5′-TTCTGT-3′), used as substitutes for ssRNA oligonucleotide sequences, were investigated using 2D ¹H−¹⁵N correlation (HSQC)[46] NMR experiments recorded at 298 K on MSU's Bruker 600 MHz solution NMR spectrometer. Freshly purified ¹⁵N-labled N-*Hv*GR-RBP1 was dialyzed against nucleic acid binding NMR buffer (25 mM sodium phosphate, 100 mM potassium chloride,

pH 6.8) in 95% H₂O/5% (v/v) D₂O, and the resulting solution concentrated to a 150 μM final protein concentration. The ssDNA fragments were dissolved in nucleic acid binding NMR buffer to stock concentrations of 1 mM. Production of N-*Hv*GR-RBP1:ssDNA NMR samples was accomplished by mixing 400 μL of the 150 μM ¹⁵N-*Hv*GR-RBP1 stock solution with 0 to 90 μL of the 1 mM ssDNA stock solutions. The resulting protein−DNA mixtures were concentrated back to 400 μL volume, equilibrated for 30 min, and then analyzed by NMR. Series of 2D ¹H−¹⁵N correlation HSQC spectra were recorded on protein:ssDNA samples corresponding to ¹⁵N-labeled N-*Hv*GR-RBP1 protein to ssDNA molar ratios of 1:0.25, 1:0.5, 1:0.75, 1:1, 1.2, and 1:1.5.

Probing the interactions of *Hv*GR-RBP1's Glycine-rich (GR) Region with the RRM Domain of *Hv*GR-RBP1 by NMR. Possible interactions between the RRM (N-*Hv*GR-RBP1) and glycine-rich (*Hv*-GR) domains of *Hv*GR-RBP1 were probed by adding progressive amounts of unlabeled N-*Hv*GR-RBP1 (0.25−1.35 mM) to a 0.5 mM ¹⁵N-labeled *Hv*-GR sample dissolved in 25 mM sodium phosphate, 100 mM potassium chloride, 95% H₂O/5% D₂O, pH 6.8, followed by recording the 2D ¹H−¹⁵N correlation HSQC spectra.

***In Vitro E. coli* Cold Shock Adaptation Assays.** Cold shock adaption assays in *E. coli* were carried out as described in refs 47 and 48 to assess whether expression of *Hv*GR-RBP1 enables *E. coli* to grow better following cold shock treatment. These experiments are analogous to the ones conducted with *Arabidopsis thaliana* glycine-rich RNA-binding proteins (*At*GRPs) that demonstrated the functional role of *At*GRPs in cold adaptation.[48−50] In these experiments, *E. coli* BL21-(DE3) cells transformed with vectors, pET46-FL-*Hv*GR-RBP1 (encoding full-length *Hv*GR-RBP1), pET46-N-*Hv*GR-RBP1 (encoding the N-terminal RRM domain of *Hv*GR-RBP1), pET32-C-*Hv*GR-RBP1 (encoding the C-terminal glycine rich domain of *Hv*GR-RBP1), pET46-FL-*Hv*GR-RBP1(F54A) (encoding a full-length version of *Hv*GR-RBP1 containing a phenylalanine to alanine substitution at residue position 54), and pET46-IsdB^N1 (encoding an unrelated protein used as control), were grown in LB medium containing 50 μg/mL ampicillin to an optical density at 600 nm (OD₆₀₀) of 0.6. This *E. coli* strain is not deficient in cold-shock proteins, and thus not the BX04 strain that is more sensitive to cold shock and used by Kim et al.[47,48] Thus, any observed effects with the *E. coli* BL21(DE3) cells are in addition to these cells' native cold-adaptation process.

Protein expression was induced using 1 mM IPTG and resulting cell cultures were allowed to grow for 2 h at 30 °C, prior to being subjected to cold shock at 10 °C for 24 h. Following a 24 h period of cold shock treatment, the cells were returned to growth conditions at 37 °C, and cell growth was monitored by recording OD₆₀₀ readings. *Hv*GR-RBP1 protein levels were assessed by SDS-PAGE using 200 μL aliquots of cell cultures obtained from the last recorded time point of growth.

***Hvgr-rbp1* Transcript Expression Following Barley Cold Treatment.** To analyze the effect of cold stress on *Hvgr-rbp1* expression, transcript levels were compared before and after chilling treatment of barley plants. Gene expression data for this analysis were obtained from the BarleyBase/PLEXdb database (http://www.plexdb.org/plex.php?database=Barley),[51] experiment BB81 (entitled "Low temperature stress in cv. Dicktoo"), deposited by L. Tommasini (University of California, Riverside). These published data were generated by growing barley plants at 20 °C for 7 days and then chilled.
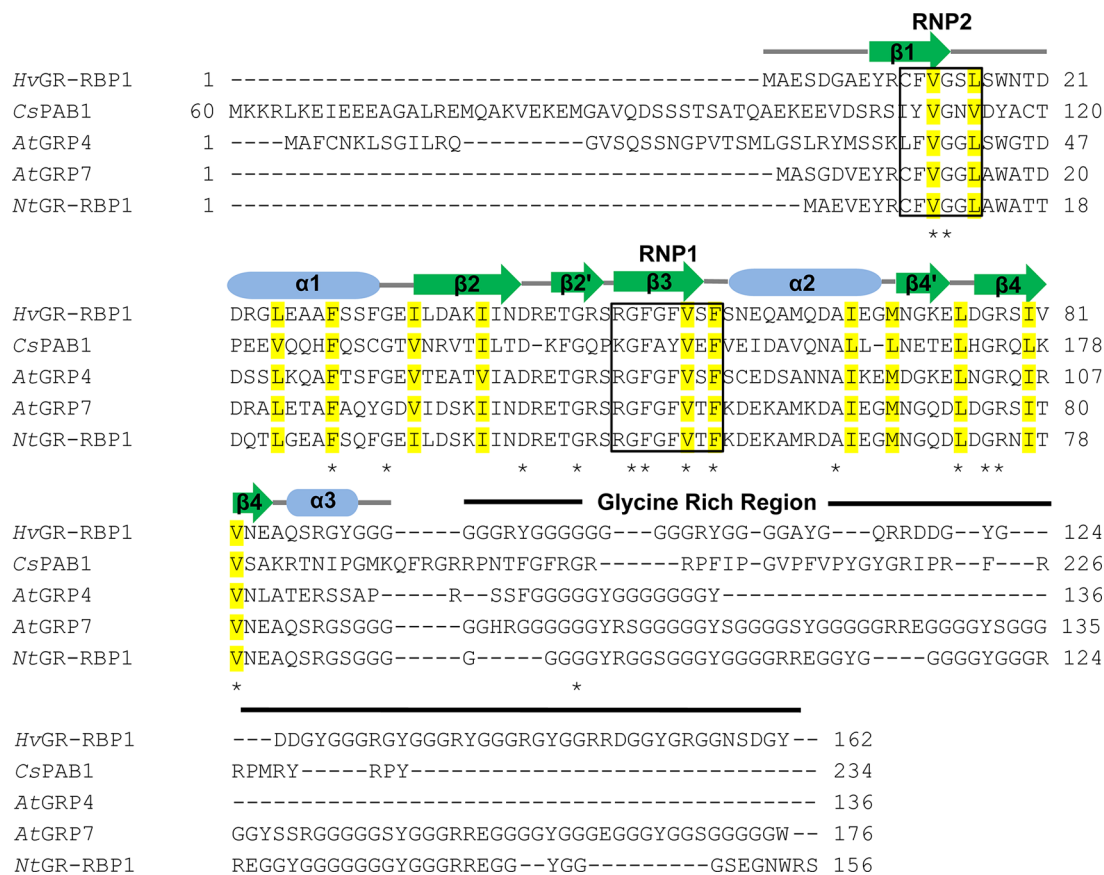
Figure 1. Multiple sequence alignment of *Hv*GR-RBP1 with homologous glycine-rich RNA-binding plant proteins. The amino acid sequences for *Hv*GR-RBP1, *Cs*PAB1 from *Citrus sinensis*, *At*GRP4 and *At*GRP7 from *Arabidopsis thaliana* and *Nt*GR-RBP1 from *Nicotiana tabacum* are displayed. Amino acid residues that are absolutely conserved in all five protein sequences are indicated by an asterisk. Conserved hydrophobic core residues are shaded in yellow. Residues that make up the RNA-binding consensus sequences RNP2 and RNP1 are indicated by boxes across all five sequences. Secondary structural elements identified in N-*Hv*GR-RBP1 are depicted above the sequence, with green arrows denoting β-strands and blue cylinders denoting a-helices. The location of the C-terminal glycine-rich (GR) region is indicated by a solid black line. The protein sequences were aligned using the Clustal Omega alignment server.

Temperature was decreased from 20 to 4 °C at a rate of 1.3 °C per hour, and plants were then kept at 4 °C (day)/2 °C (night) for 5 days. Leaves were harvested and analyzed using the Affymetrix Barley1 GeneChip.[52] RMA-normalized data[53] for contig17116_at (representing *Hvgr-rbp1* transcript; three replicates) were downloaded from BarleyBase, and analyzed for significance using a Student's *t* test (two-sided; two independent samples assuming equal variance) using Microsoft Excel for Windows (Microsoft Corporation, Redmond, WA).

■ RESULTS

Three Dimensional Structure of *Hv*GR-RBP1. Full-length *Hv*GR-RBP1 is composed of 162 amino acids. Sequence analysis indicated that the N-terminal region of *Hv*GR-RBP1 (residues 1−92) shares sequence homology with proteins containing RNA-recognition motifs (RRMs),[15,20−22] while the C-terminal region (residues 93−162) is enriched in glycine residues and contains a series of (GGR/RGG) repeats that are commonly found in glycine-rich RNA-binding proteins from plants.[13] Full-length *Hv*GR-RBP1 is very similar in sequence (65% sequence identity) to the *Arabidopsis thaliana* glycine-rich RNA-binding protein *At*GRP7, which has been found to regulate numerous developmental and environmental adaptation processes in *Arabidopsis*,[54,55] and to the *Nicotiana tabacum*

*Nt*GR-RBP1 protein (71% sequence identity) (Figure 1), thus is in all likelihood an ortholog of these proteins.

Initial *in vitro* studies of full-length *Hv*GR-RBP1 (FL-*Hv*GR-RBP1) indicated that the C-terminal glycine-rich region is easily degraded following purification from cell extracts, whereas the N-terminal RRM domain (residues 1−92) is more resistant to protease degradation (data not shown). Further and as previously reported,[26] full-length *Hv*GR-RBP1 is prone to aggregation and precipitation at the millimolar concentrations and buffer conditions required for multidimensional heteronuclear (^{1}H, ^{15}N, ^{13}C) NMR analysis. At lower protein concentrations, the 2D-^{1}H−^{15}N HSQC spectra of ^{15}N-labeled FL-*Hv*GR-RBP1 exhibited significantly broadened ^{1}H/^{15}N amide resonances positioned within the central "random coil" chemical shift region (i.e., ^{1}H ∼ 8 ppm; ^{15}N ∼ 120 ppm) of the HSQC spectrum, and broader NMR resonances for signals outside of this random coil region than is expected for a protein of ∼18 kDa (Figure 2A). These data would indicate that under these conditions the protein aggregates and nonspecific intermolecular association takes place. Interestingly, this resonance line-broadening phenomenon appears to be dependent on pH and temperature. Raising the temperature from 298 to 303 K resulted in 2D ^{1}H−^{15}N HSQC spectra with narrower resonance line-widths and improved resolution of ^{1}H/^{15}N amide signals (Figure 2B).
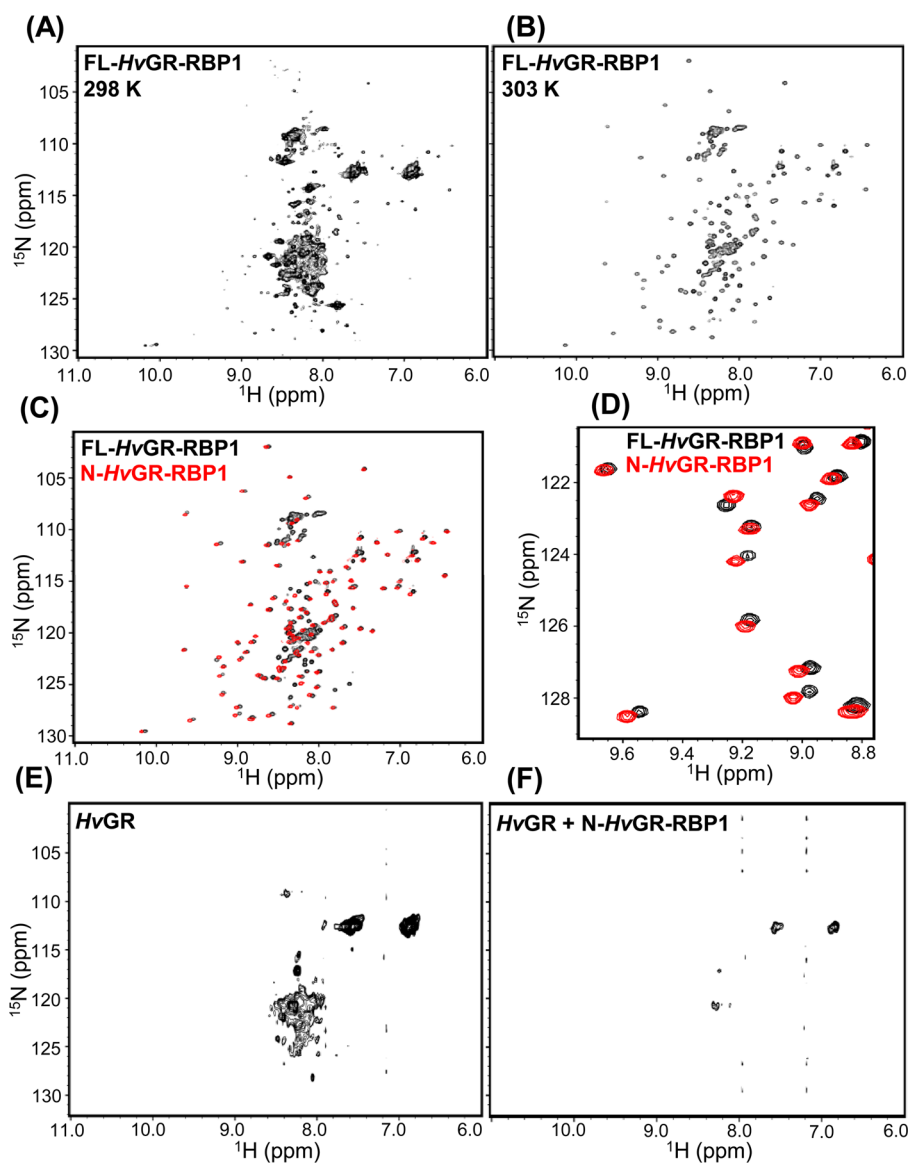
Figure 2. Comparison of various 2D ^{1}H–^{15}N-HSQC spectra showing interactions between the RRM and GR domains of *Hv*GR-RBP1. (A,B) Effect of temperature on FL-*Hv*GR-RBP1: (A) 2D ^{1}H–^{15}N-HSQC spectra recorded at 298 K, pH 6.2, and 250 μM protein concentration, displaying severely broadened resonances and resulting in the observation of two resonances for the indole ^{1}H/^{15}N signal of Trp18. Altogether, these observations are indicative of intermolecular association. (B) 2D ^{1}H–^{15}N-HSQC spectra recorded at 303 K, pH 6.2, displaying sharp, well-resolved resonances with line widths consistent with an ~18 kDa protein. (C) Overlays of FL-*Hv*GR-RBP1 (black) and N-*Hv*GR-RBP1 (red) recorded at pH 6.2 and temperature of 303 K showing shifted NMR signal in the presence or absence of the glycine-rich (GR) GR region in *Hv*GR-RBP1. (D) Expanded view of a spectral region of overlaid 2D ^{1}H–^{15}N HSQC spectra of FL-*Hv*GR-RBP1 (black) and N-*Hv*GR-RBP1 (red), indicating notable chemical shift changes of the ^{1}H/^{15}N NMR signal arising from *Hv*GR-RBP1's RRM domain. (E) 2D ^{1}H–^{15}N-HSQC spectrum of the glycine-rich domain (*Hv*GR) of *Hv*GR-RBP1. ^{15}N-labeled *Hv*GR (residues 93−162) was produced using a pET46 expression vector, and the resulting 2D ^{1}H–^{15}N NMR spectrum was recorded at pH 6.2 and temperature of 298 K. (F) 2D ^{1}H–^{15}N-HSQC spectrum of ^{15}N-labeled *Hv*GR upon addition of unlabeled N-*Hv*GR-RBP1.

Comparing the 2D ^{1}H–^{15}N correlation (HSQC) spectra of ^{15}N-labeled FL-*Hv*GR-RBP1 and N-*Hv*GR-RBP1 (RRM domain only) recorded under identical NMR conditions at pH 6.2 and temperature of 303 K (Figure 2C and D) revealed small but significant differences in the chemical shift positions of several resonances originating from the RRM domain of *Hv*GR-RBP1.

These data indicate that under these conditions, the GR region of *Hv*GR-RBP1 interacts with the RRM domain of the protein. Interestingly, further increases in pH (from 6.2 to 7.2) decreased these chemical shift differences, resulting in 2D ^{15}N–^{1}H HSQC spectra that look very similar to the one of

RRM-only N-*Hv*GR-RBP1 with a corresponding disappearance of ^{1}H/^{15}N signals originating from the *Hv*GR region (see Supporting Information Figure S4). Similarly, truncation of the 25 and 50 most C-terminal residues of *Hv*GR-RBP1 glycine-rich domain (137-*Hv*GR-RBP1 and 112-*Hv*GR-RBP1, respectively) eliminated ^{1}H/^{15}N chemical shift differences for NMR signals corresponding to the RRM domain of *Hv*GR-RBP1 (Supporting Information Figure S5). These data suggest that the interactions between the RRM and GR domains of *Hv*GR-RBP1 either require the complete *Hv*GR sequence, or that these interdomain interactions are specifically mediated by the 25 most C-terminal residues of *Hv*GR.
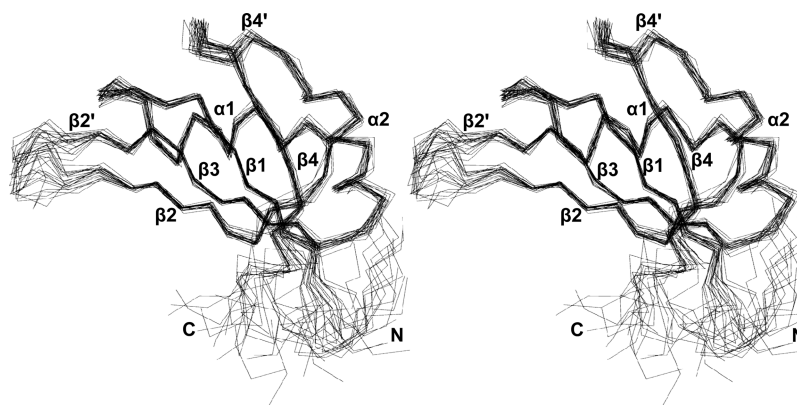
Figure 3. Structural ensemble of N-*Hv*GR-RBP1 conformers as determined by multidimensional solution NMR. The family of 20 lowest energy conformers depicting the 3D structure of N-*Hv*GR-RBP1 (Met1-Gly92) is shown in "walleyed" stereo view. Black lines represent the backbone atom (N, Cα, and C′) trace of each polypeptide chain of the 20 conformers. Secondary structural elements are labeled β1 (residues 10−14), α1 (residues 22−32), β2 (residues 36−43), β2′ (spanning residues 47−49), β3 (residues 51−57), α2 (residues 60−70), β4′ (residues 72−75), β4 (residues 78−84), and α3 (residues 86−89). The structural ensemble figure was generated using PYMOL graphics software.

A 2D ^{1}H−^{15}N HSQC spectrum recorded at a pH of 6.8 and temperature of 298 K of an ^{15}N-labeled glycine-rich (*Hv*GR) protein sample (Figure 2E) reveals that the glycine-rich domain of *Hv*GR-RBP1 is unstructured in solution, displaying only broad resonances in the central "random coil" region of the spectrum similar to that shown in Figure 2A. Titration of unlabeled N-*Hv*GR-RBP1 into an ^{15}N-labeled glycine-rich (*Hv*GR) protein does perturb the spectral characteristics of the NMR resonances arising from ^{15}N-labeled *Hv*GR (Figure 2F). Spectral changes taking place upon addition of unlabeled N-*Hv*GR-RBP1 to ^{15}N-*Hv*GR suggest that the two protein domains can interact *in vitro* in trans, although the biological significance of these interactions is unclear. Taken together, these data indicate that the glycine-rich GR region of *Hv*GR-RBP1 can participate in intra- and intermolecular interactions with the protein RRM domain, although these protein−protein interactions appear to be weak. In contrast, N-*Hv*GR-RBP1 composed solely of the protein RRM domain and spanning residues 1−92 is well-folded and amenable to detailed structural determination by NMR.

Solution Structure of N-*Hv*GR-RBP1. The 3D solution structure of N-*Hv*GR-RBP1 was solved using well-established, heteronuclear (^{1}H, ^{15}N, ^{13}C), multidimensional solution NMR experiments and standard computational torsion angle simulated annealing protocols. Resonance assignments of backbone and side-chain atoms were nearly complete (>97%) with only the ^{1}H/^{15}N backbone amide resonances of V55 unobservable. The final 3D structure of N-*Hv*GR-RBP1 was computed using 683 interproton (^{1}H−^{1}H) NOE, 83 dihedral angle, and 74 hydrogen bond distance restraints, as shown in Table 1 which summarizes the NMR experimental constraints used and resulting structural statistics. An overlay of the Cα backbone traces of the final set of 20 low energy conformers depicting the ensemble of N-*Hv*GR-RBP1 structures is shown in Figure 3. These conformers exhibit excellent bond and stereochemical properties, with no NOE-derived distance violations greater than 0.5 Å or dihedral angle violations greater than 5°. Dihedral angle analysis indicates that all residues within the structurally ordered region (residues 10−84) of N-*Hv*GR-RBP1 have ϕ and ψ dihedral angle values that are within the allowed ranges of the Ramachandran plot. Residues 10−84 of N-*Hv*GR-RBP1 are well ordered and converge into a well-folded structure with a pairwise backbone

heavy atom RMSD of 0.66 Å (Table 1). In contrast, the N- and C-termini of the protein (residues 1−9 and 85−92) are less well-defined.

The solution structure of N-*Hv*GR-RBP1 adopts a canonical RRM structural fold[21,22] consisting of a four-stranded antiparallel β-sheet and two α-helices arranged in a $β_1α_1β_2β_3α_2β_4$ secondary structural topology (Figure 4). The two α-helices ($α_1$ and $α_2$) are positioned on the same side of the protein almost at a right angle to each other, as has been seen in other RRM structural folds.[22] The three loops connecting the various β-strands and α-helices all appear to be well-defined, with two loops (loops 3 and 5) incorporating
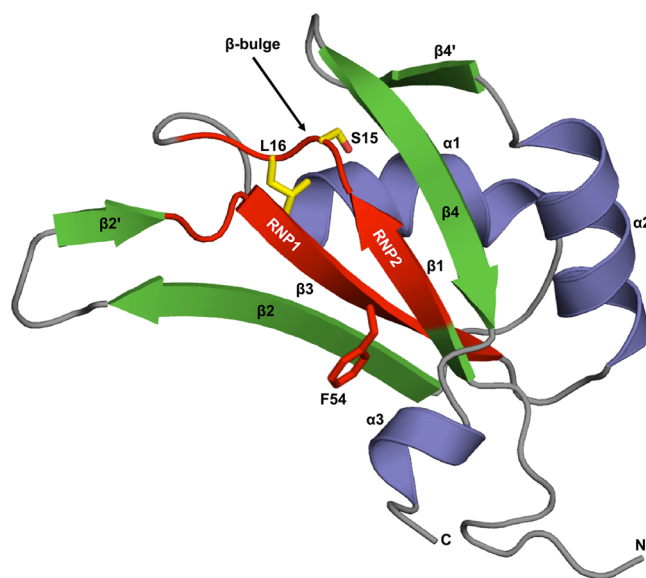

Figure 4. Ribbon representation of a representative N-*Hv*GR-RBP1 structural conformer from the ensemble of 20 lowest energy NMR structures of N-*Hv*GR-RBP1. The secondary structure elements are colored in green (β-strands) and blue (α-helices). Side chains of residues Ser 15 and Leu 16 contributing to formation of a β-bulge within the structure are shown as solid stick representations, and the β-bulge is indicated by an arrow. Locations of RNP1 and RNP2 are indicated (red) and phenylalanine 54 (F54), site of the phenylalanine to alanine amino acid substitution, is shown as a solid stick (red) on β-strand 3.

two additional short β-strands to create two β-hairpin structures (β2/β2′ and β4/β4′) spanning the structural elements β2 and β3 and α2 and β4, respectively. Such hairpin structures are not typically observed in other RRM structural folds.[20−22,56]

The hydrophobic core of the protein comprises several conserved hydrophobic residues (highlighted in yellow in Figure 1), which are located primarily within the $\beta_1\alpha_1\beta_2\beta_3$ region of the protein. This region also includes the two conserved RNA-binding consensus sequences RNP2 and RNP1[22] that project the aromatic side chains of Phe12, Phe52, and Phe54 from the plane formed by the two central β-strands β_3 and β_1, respectively, priming these residues for base stacking interactions with potential RNA targets.[56] Interestingly, the hydrophobic packing of the side chain of Leu16 into the hydrophobic core results from a sharp curvature of the polypeptide backbone chain formed by a β-bulge created by Ser15 and Leu16 within the β1-loop1 region (Figure 4). RRM-containing proteins with a β-bulge have been observed previously, but typically, the bulge is located within the β2 strand of the proteins (see, for example, the RNA-binding domains, RBD1 and RDB2, of U1A, Sex lethal, and hnRNP1 D0[57]).

Lastly, the N- and C-termini (i.e., residues 1−9 and 85−92, respectively) of N-*Hv*GR-RBP1 are positioned on the same side in the 3D structure of the protein. The N-terminal segment is largely disordered and most likely highly flexible, as judged by the intensity of the NMR signals, the presence of random coil ^{1}H, ^{15}N, and ^{13}C chemical shifts, the lack of observable amides protected from ^{1}H/^{2}H solvent exchange, and the scarcity of interproton NOE-based distance restraints for residues located within this region. Residues in the C-terminal end of N-*Hv*GR-RBP1 exhibit similar characteristics, except for the formation of a short α-helical turn (α3) within residue stretch 86−89 (Figure 4).

Structural Comparison of N-*Hv*GR-RBP1 with Other RRM-Containing Proteins. The DALI[41] and SSM[58] databases were utilized to search for structural homologues of the RRM domain of *Hv*GR-RBP1. Homology search results reveal that RRM of N-*Hv*GR-RBP1 is most structurally similar to other eukaryotic RRM domains, including the RRM2 domain of the T-cell restricted intracellular antigen-1 (TIA-1) protein (PDB ID = 3BS9, Z-score = 12.7, RMSD = 1.5 Å, 43% sequence identity),[59] and the RRM1 domain of the polyadenylate-binding protein 1 (PABP1) (PDB ID = 4F02, Z-score = 12.2, RMSD = 2.4 Å, 24% sequence identity),[60] both of which are involved in post-transcriptional regulation of gene expression including pre-mRNA splicing in the nucleus and mRNA translation in the cytoplasm (see Supporting Information Figures S1 and S2).

Restricting our DALI structural homology search to other RRM-containing plant proteins yielded the closest structural homology to the RRM domain of the *Nicotiana tabacum* glycine-rich RNA-binding protein 1, *Nt*GR-RBP1 (PDB ID = 4C7Q, Z-score = 11.1, RMSD = 2.6 Å, 72% sequence identity), suggested to function as an RNA chaperone,[24] and the RRM domain of the poly(A) binding protein 1 from *Citrus sinensis*, CsPABP1 (PDB ID = 2M70, Z-score = 9.0, RMSD = 3.0 Å, 26% sequence identity),[23] suggested to associate with the poly(A) tail of mRNA and, similarly to cytoplasmic PABP proteins, to regulate the translation of polyadenylated mRNAs and mRNA decay[61,62] (Figure 5A,B). Sequence analysis also revealed that the amino acids within the putative nucleotide-binding site of *Hv*GR-RBP1, *Nt*GR-RBP1, and *At*GRBP7 are
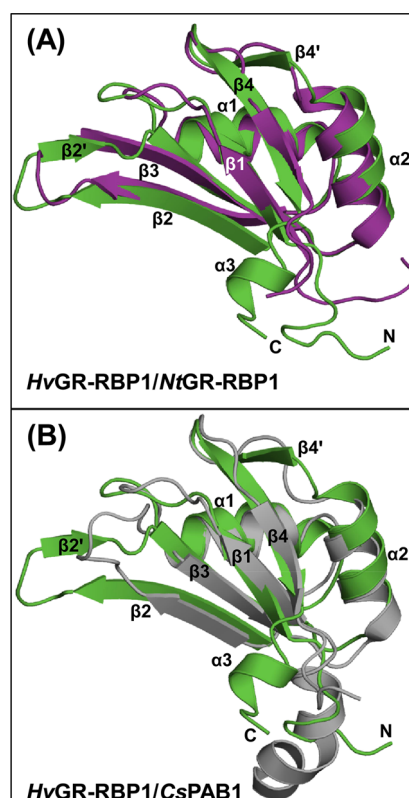

Figure 5. Overlay of the 3D structure of N-*Hv*GR-RBP1 (in green) (A) with that of *Nt*GR-RBP1 (colored in cyan, PDB entry 4C7Q) from *Nicotiana tabacum*, and (B) with the structure of *Cs*PAB1 (colored in gray, PDB entry 2M70) from *Citrus sinensis*. These structural overlays highlight the structural similarity of *Hv*GR-RBP1 to these two other RRM-containing proteins from plants. The three-dimensional structures were aligned using the SSM program of the COOT software and displayed using PYMOL.

identical, suggesting that all three orthologs may bind similar nucleic acid target sequences (Figure 6).

***In Vitro* Assays Testing the Ability of *Hv*GR-RBP1 to Bind to Various Nucleic Acid Sequences.** *In vitro* gel electrophoretic mobility shift assays (EMSAs) were performed using single-stranded RNA (ssRNA), single-stranded DNA (ssDNA), and double-stranded DNA (dsDNA) templates to assess the nucleic acid binding capabilities of *Hv*GR-RBP1. Since *At*GRP7 has been reported to bind to and regulate the splicing of its own pre-mRNA transcript, full-length genomic *Hvgr-rbp1* was used to evaluate whether *Hv*GR-RBP1 can bind to its own pre-mRNA transcript. Results of FL-*Hv*GR-RBP1 binding to *Hvgr-rbp1* ssRNA are shown in Figure 7A. In general, increasing concentrations of FL-*Hv*GR-RBP1 (0−1 μM) protein shifted the electrophoretic mobility of the *Hvgr-rbp1* ssRNA band. Addition of N-*Hv*GR-RBP1 (which corresponds to the N-terminal RRM domain only of *Hv*GR-RBP1) to the *Hvgr-rbp1* ssRNA template resulted in no electrophoretic mobility shift of the ssRNA transcript (Figure 7B).

Similarly, truncated constructs of *Hv*GR-RBP1 including 112-*Hv*GR-RBP1 and 137-*Hv*GR-RBP1 (the latter lacking only the 25 C-terminal residues of the full-length protein) also resulted in no band shift (Figure 7C). These data suggest that no interactions take place between these protein products and ssRNA under the conditions of these *in vitro* EMSA assays. The lack of ssRNA binding using either 112-*Hv*GR-RBP1 or 137-
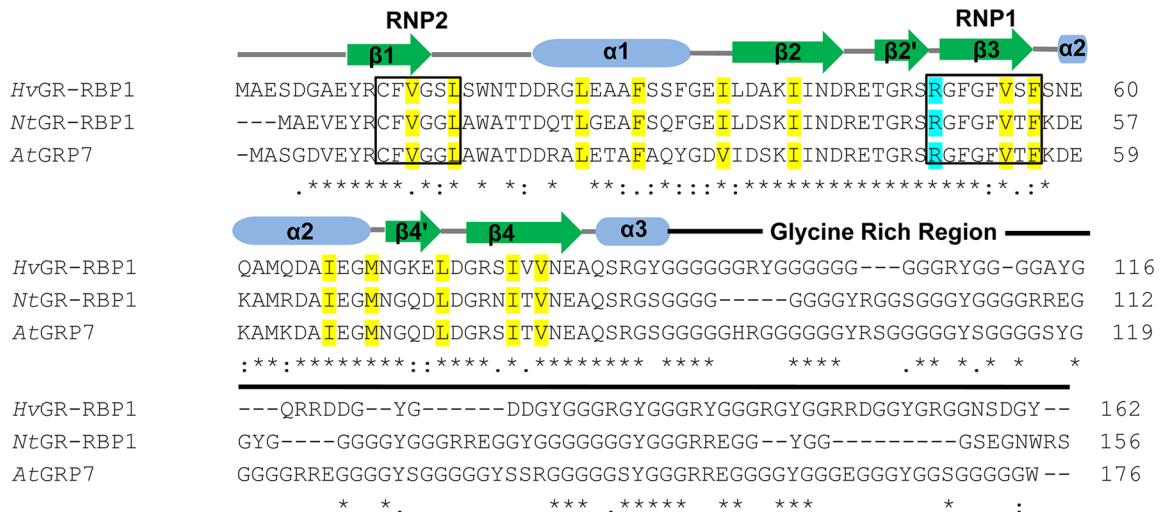
```
                        RNP2                                    RNP1
          ──────→  β1 ────→   ◁═ α1 ═▷  ──→ β2 ──→  β2' ─→ β3 ──→  α2
HvGR-RBP1  MAESDGAEYRCFVGSLSWNTDDRGLEAAFSSFGEILDAKIINDRETGRSRGFGFVSFSNE   60
NtGR-RBP1  ---MAEVEYRCFVGGLAWATTDQTLGEAFSQFGEILDSKIINDRETGRSRGFGFVTFKDE   57
AtGRP7     -MASGDVEYRCFVGGLAWATDDRALETAFAQYGDVIDSKIINDRETGRSRGFGFVTFKDE   59
            .*******.:* * *: * **..:*:::*:****************.*.:*

              ◁═ α2 ═▷   β4' ─→   β4 ───→  ◁═ α3 ═▷ ── Glycine Rich Region ──
HvGR-RBP1  QAMQDAIEGMNGKELDGRSIVVNEAQSRGYGGGGGGGRYGGGGGG---GGGRYGG-GGAYG  116
NtGR-RBP1  KAMRDAIEGMNGQDLDGRNITVNEAQSRGSGGGG-----GGGGYRGGSGGGYGGGGRREG  112
AtGRP7     KAMKDAIEGMNGQDLDGRSITVNEAQSRGSGGGGGHRGGGGGGYRSGGGGGYSGGGGSYG  119
            :**:*********::****.*.******** ****   ****   .** *.* *   *

HvGR-RBP1  ---QRRDDG--YG------DDGYGGGRGYGGGRYGGGRGYGGRRDGGYGRGGNSDGY--  162
NtGR-RBP1  GYG----GGGGYGGGRREGGYGGGGGGGYGGGRREGG--YGG---------GSEGNWRS  156
AtGRP7     GGGGRREGGGGYSGGGGGYSSRGGGGGSYGGGRREGGGGYGGGEGGGYGGSGGGGGW--  176
             *  *.       *** .***** **  ***        *    :
```

Figure 6. Amino acid sequence alignment of *Hv*GR-RBP1 with its most closely related plant homologues *At*GRP7 and *Nt*GR-RBP1. Conserved hydrophobic core residues are shaded in yellow. Fully conserved amino acid residues are highlighted by an asterisk. Residues that are very similar in chemical properties, but not identical, are denoted by a colon, and residues that are weakly similar are indicated by a dot. Absence of a symbol denotes that there is no common property between the amino acids. The Arg 49 residue (highlighted in blue) of *At*GRP7 has been identified as being critical for the alternative mRNA splicing function of *At*GRP7.[8] A structurally equivalent residue (Arg 50) is found at that same location in the 3D structure of *Hv*GR-RBP1 (highlighted in blue), and is part of the protein RNP1 consensus sequence. This suggests that R50 in *Hv*GR-RBP1 may be important for this protein to function in alternative splicing.

*Hv*GR-RBP1 protein constructs indicates that the complete C-terminal glycine-rich (GR) region of full-length *Hv*GR-RBP1 is necessary to detect protein binding to ssRNA under the conditions of these *in vitro* nucleic acid binding experiments.

When the different *Hv*GR-RBP1 constructs were incubated with either dsDNA or ssDNA (not shown) coding for the full-length *Hvgr-rbp1* gene, no visible shift in gel mobility was observed (Figure 7D), suggesting that *Hv*GR-RBP1 binds preferentially to ssRNA. The ability of N-*Hv*GR-RBP1 and FL-*Hv*GR-RBP1 to bind to an ssRNA affinity chromatography column composed of RNA isolated from barley plant leaf samples was also tested. As observed with EMSA experiments, we found that N-*Hv*GR-RBP1 could not be retained on the ssRNA-bound affinity chromatography column, whereas FL-*Hv*GR-RBP1 was retained on the column and could be eluted from the column using increasing ionic strength KCl salt solutions. The interaction of full-length *Hv*GR-RBP1 with ssRNA, however, was determined to be nonspecific, as similar binding of full-length *Hv*GR-RBP1 was observed with unrelated RNA transcribed from *E. coli* genomic DNA (data not shown). Lastly, to establish whether the C-terminal GR domain of *Hv*GR-RBP1 is sufficient to bind to ssRNA *in vitro*, a fusion protein comprising thioredoxin and the GR domain of *Hv*GR-RBP1 was prepared and tested for its ability to bind to an unrelated ssRNA construct derived from a mRNA sequence coding for a green fluorescent protein (GFP). As anticipated from earlier observations, the fusion protein containing the GR domain of *Hv*GR-RBP1 resulted in an electrophoretic mobility band shift of this ssRNA construct (Figure 7E), suggesting that the glycine-rich (GR) domain of *Hv*GR-RBP1 is sufficient to modulate nonspecific ssRNA binding.

NMR Analysis of N-*Hv*GR-RBP1 Binding to ssDNA. Although the N-terminal RRM domain of *Hv*GR-RBP1 did not bind ssRNA in the *in vitro* EMSA assays conducted, these results are insufficient to unambiguously establish whether the RRM domain of *Hv*GR-RBP1 is incapable of interacting with ssRNA. Lack of RNA binding would be surprising, as other

isolated RRMs from GR-RBP proteins have been shown to bind, albeit very weakly, to single-stranded RNA targets.[20] Evidence from the literature would thus suggest that the ssRNA binding affinity of N-*Hv*GR-RBP1 (containing only the RRM domain of *Hv*GR-RBP1) may be too weak to be observable using the described *in vitro* EMSA experiments. Recently, a 6-nt DNA sequence (5′-TTCTGG-3′) has been used as a proxy for a 6nt ssRNA sequence identified as a putative nucleic acid binding site for *Nt*GR-RBP1 based on sequence similarity with nucleotide sequences present within the 3′-UTR region of *At*grp7 and *Nt*gr-rbp1 pre-mRNA.[24] Analysis of the genomic sequence of *Hvgr-rbp1* reveals the presence of two homologous sequences, 5′-TTCTGA-3′ and 5′-TTCTGT-3′, one located in the 3′-UTR region of *Hvgr-rbp1* pre-mRNA, and the second located upstream near the 5′-end of the intron. The locations of these sequences in the *Hvgr-rbp1* gene are analogous to *At*GRP7 nucleotide binding sites identified in *At*grp7 pre-mRNA (Figure 8).

These observations led us to investigate whether or not the RRM domain of *Hv*GR-RBP1 can bind to 6-nucleotide ssDNA sequences corresponding to segments of the 3′-UTR and intronic regions of *Hvgr-rbp1* pre-mRNA. Subsets of 2D ^{1}H−^{15}N correlation HSQC spectra resulting from these titration experiments are shown in Figure 9. In the absence of the nucleotide ssDNA ligand, the 2D ^{1}H−^{15}N HSQC spectrum of ^{15}N-labeled N-*Hv*GR-RBP1 is well-resolved and similar to the one reported in ref 26 and in Figure 2C of the present manuscript. Progressive titration of unlabeled 5′-TTCTGA-3′ up to a 1:1.5 molar ratio of ^{15}N-labeled N-*Hv*GR-RBP1 to ssDNA elicited small but noticeable spectral changes in the 2D ^{1}H−^{15}N HSQC spectrum of N-*Hv*GR-RBP1 (Figure 9A). Most notable were changes in amide ^{1}H/^{15}N chemical shifts of residues F12, W18, N19, T20, F52, and Q86, residues primarily within or adjacent to RNP1 and RNP2 consensus RNA-binding sequence sites. These residues correspond to the RNA-binding site of the RRM motif of
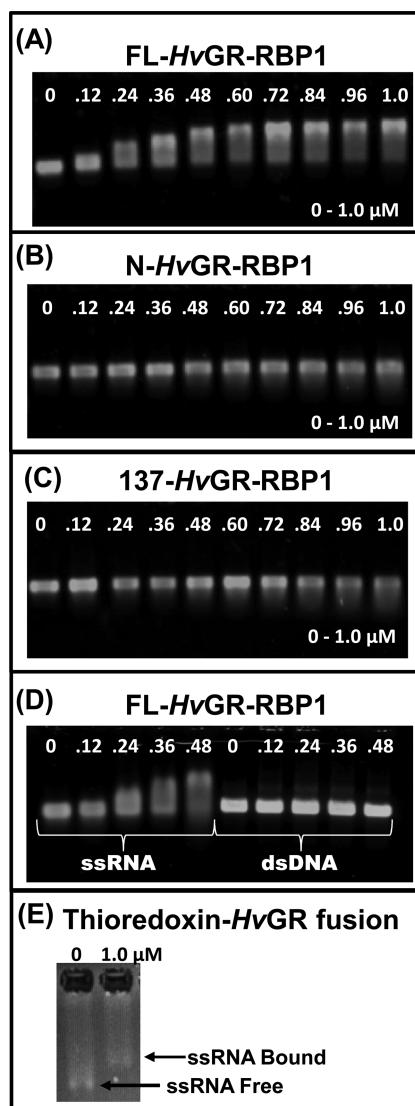
Figure 7. Gel electrophoretic mobility shift assays (EMSAs) probing the interaction of HvGPRBP1 protein constructs with single-stranded RNA (ssRNA) and double-stranded DNA (dsDNA) templates. Protein concentrations are indicated above each lane of the gels. (A) ssRNA produced from *in vitro* transcription and mixed in with full-length HvGR-RBP1 results in a band shift in electrophoretic mobility indicating that full-length HvGR-RBP1 binds ssRNA. (B) Deletions of the protein's C-terminal glycine-rich domain (N-HvGR-RBP1) results in a loss of ssRNA binding under the conditions of the EMSA assay. (C) Deletion of the 25 most C-terminal residues of the glycine-rich domain of HvGR-RBP1 (137-HvGR-RBP1) also results in loss of ssRNA binding (D, right side). Mixing of FL-HvGR-RBP1 with dsDNA has no effect on gel electrophoretic mobility, while in contrast (D, left side), an electrophoretic mobility band shift is observed when ssRNA is mixed with FL-HvGR-RBP1 under identical conditions. (E) A fusion protein comprising thioredoxin and the C-terminal glycine-rich domain of HvGR-RBP1 (Thioredoxin-HvGR) can bind a GFP-coding ssRNA.

HvGR-RBP1 which includes the RNA-binding consensus sequences RNP1 and RNP2 (Figures 4 and 9C–D).

Similar ^{1}H/^{15}N chemical shift changes were observed in the 2D ^{1}H–^{15}N HSQC spectrum of ^{15}N-labeled N-HvGR-RBP1 upon titration of the 6-nt fragment 5′-TTCTGT-3′ whose sequence is part of the 3′-UTR region of HvGR-RBP1's pre-mRNA. Moreover, the magnitude of these chemical shift
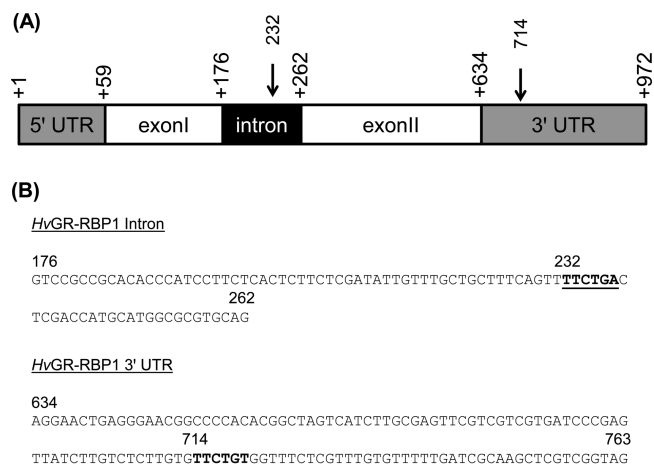

Figure 8. (A) Schematic representation of the genomic DNA sequence of Hvgr-rbp1. 5′- and 3′-untranslated regions (5′UTR and 3′UTR) are indicated by gray rectangles, exons 1 and 2 by white-shaded rectangles, and the intron by a solid black rectangle, with nucleotide positions indicated above. Locations of the CTG binding elements are indicated with solid arrows. (B) Partial DNA nucleotide sequences corresponding to the intron and 3′UTR region of the Hvgr-rbp1 gene are shown to indicate the potential CTG binding elements (bold and underlined) that may be recognized and bind specifically to HvGR-RBP1 when transcribed to ssRNA.

changes is similar to what is observed upon titration of the 6-nt fragment 5′-TTCTGG-3′, which had been used in nucleic acid binding experiments of NtGR-RBP1.[24] These data thus indicate that differences within the last nucleotide position of these 6 nt ssDNA fragments contribute little if anything to the nucleotide binding specificity of the RRM domain.

To assess the specificity of these single-stranded 6-nucleotide binding interactions, we also investigated the capability of N-HvGR-RBP1 to bind to a randomized 6-nt fragment 5′-CTGTTG-3′, which retains the CTG binding element identified in the NtGR-RBP1 studies,[24] but is altered with respect to the nature of the flanking nucleotides. Titration of this ssDNA fragment into an ^{15}N-labeled N-HvGR-RBP1 protein sample resulted in the observation of smaller ^{1}H/^{15}N chemical shift changes in resulting 2D-^{1}H–^{15}N HSQC spectra of ^{15}N-labeled N-HvGR-RBP1 in complex with this ssDNA (Figure 9B). The equilibrium dissociation constant (K_d) for binding of this randomized 5′-CTGTTG-3′ ssDNA to ^{15}N-labeled N-HvGR-RBP1 was determined to be ∼550 μM, much higher than the K_d values ranging from ∼4 to 43 μM for the other ssDNA ligands (see Supporting Information Table S1). These chemical shift perturbation experiments thus indicated that the nucleotides adjacent to the CTG binding element are important modulators of the interactions of N-HvGR-RBP1 with single-stranded 6-nucleotide ssDNA targets. Overall, these results demonstrate that the N-terminal RRM domain of HvGR-RBP1 can interact weakly with ssDNA fragments. The high nucleotide sequence identity and location of these nucleotide fragments within the 3′UTR or intronic region of the pre-mRNA of Hvgr-rbp1 suggest that HvGR-RBP1 may regulate self-splicing of its own mRNA transcript, similar to what has been observed for *Arabidopsis thaliana* AtGRP7.[63,64]

Effect of Cold Stress on Hvgr-rbp1 Gene Expression. Interestingly, in addition to their role in plant development and genome organization, glycine-rich RNA-binding proteins have been shown to play a key role in the response of plants to
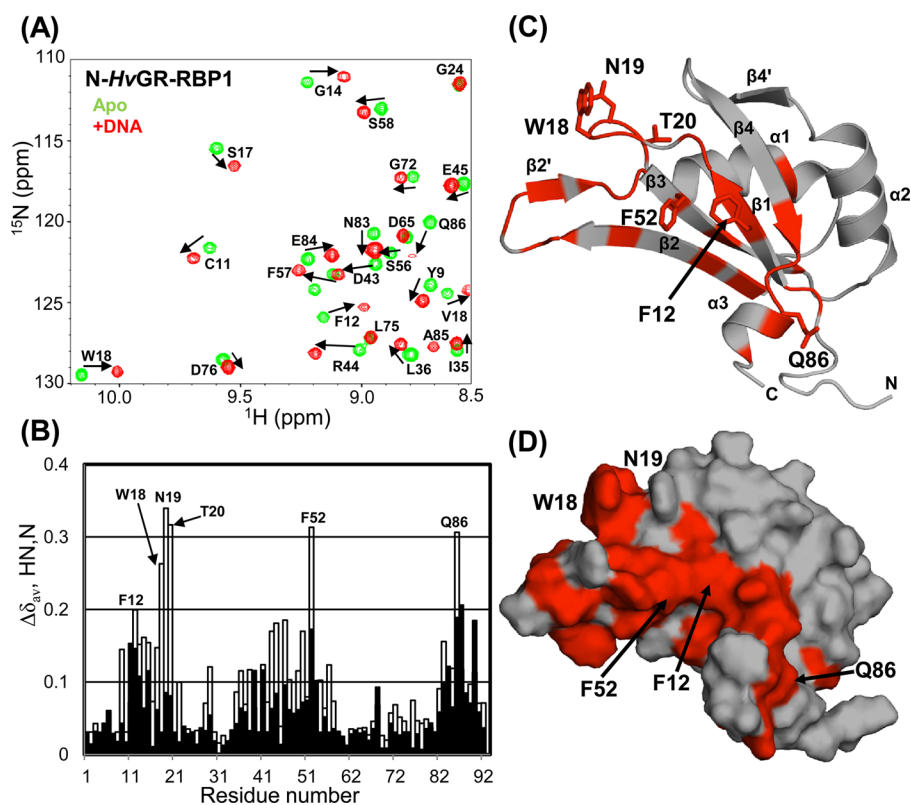
Figure 9. (A) Expanded view of an overlay of 2D $^1H-^{15}N$ correlation HSQC spectra displaying the change in $^1H/^{15}N$ chemical shifts of several amide resonances upon titration of ssDNA fragment 5′-TTCTGT-3′ into an ^{15}N-labeled N-HvGR-RBP1 NMR sample. Resonance assignments are shown along with arrows indicating the directions of the $^1H/^{15}N$ chemical shift changes. Contour levels corresponding to the location of the $^1H/^{15}N$ resonances of N-HvGR-RBP1 in the absence of ssDNA are shown in green, while final chemical shift positions following the addition of ssDNA are shown in red. (B) Plot of the magnitude of $^1H/^{15}N$ chemical shift changes ($\Delta\delta_{av}$, H^N/N) observed in ^{15}N-labeled N-HvGR-RBP1 upon ssDNA binding as a function of residue number. Chemical shift changes observed for ^{15}N-labeled N-HvGR-RBP1 bound to ssDNA fragment 5′-CTGTTG-3′ are indicated by solid black bars, while those observed for ^{15}N-labeled N-HvGR-RBP1 bound to DNA fragment 5′-TTCTGT-3′ are shown in white bars. The reported ($\Delta\delta_{av}$, H^N/N) values represent weighted averages of the ^{15}N and $^1H^N$ chemical shifts of each amide and are calculated as follows: $\Delta\delta_{av} = (0.5[\Delta\delta(H^N)^2 + [0.2\Delta\delta(^{15}N)]^2])^{1/2}$, where $\Delta\delta(H^N)$ and $\Delta\delta(^{15}N)$ are the chemical shift differences of the amide proton (H^N) and amide nitrogen (^{15}N), respectively. (C) Ribbon representation of the 3D structure of N-HvGR-RBP1 colored in gray. Residues whose amides experience chemical shift perturbations ≥0.1 ppm ($\Delta\delta_{av}$) upon ssDNA binding (i.e., Y9, F12, V13, G14, S15, S17, W18, N19, T20, F29, D22, L36, A38, I41, D43, R44, T46, G47, R48, S49, R50, F52, G53, F54, F57, V82, N83, E84, A85, Q86, S87, G89, and Y90) are colored in red. Side chains of amino acids whose $^1H/^{15}N$ amides experience chemical shift changes ≥0.2 ppm ($\Delta\delta_{av}$) upon ssDNA binding are highlighted as stick representations and labeled. (D) Gray surface representation of N-HvGR-RBP1, with residues involved in nucleic acid binding interactions, as monitored in the NMR N-HvGR-RBP1/DNA titration study colored in red. Residues whose $^1H/^{15}N$ amide chemical shifts changed by ≥0.2 ppm ($\Delta\delta_{av}$) are labeled.

environmental stresses.[12,13] In particular, AtGRP7 has been shown to function as an RNA chaperone during the cold adaption process of *Arabidopsis thaliana* plants.[48,50] To explore the effect of cold stress on *Hvgr-rbp1* gene expression, transcript data retrieved from the BarleyBase/PLEXdb database (experiment BB81) in which barley plants were subjected to a 4 °C chilling treatment were compared to transcript levels before treatment. It can be seen that *Hvgr-rbp1* transcript levels increased following the chilling treatment (Supporting Information Figure S3) indicating this gene is induced by cold stress.

Influence of HvGR-RBP1 on E. coli Growth Following Cold Shock. To examine whether HvGR-RBP1 functions as an RNA chaperone in response to cold stress, similar to what has been demonstrated for the glycine-rich RNA-binding protein atRZ-1a of *Arabidopsis thaliana*,[47,48] we investigated the growth of *E. coli* cells that were heterologously expressing FL-HvGR-RBP1, FL-HvGR-RBP1(F54A), IsdB[N1] (an unrelated control protein), or truncated constructs containing either the N-terminal RRM domain (N-HvGR-RBP1) or the C-terminal

glycine rich region of HvGR-RBP1 (HvGR) following cold shock stress. *E. coli* cells were grown to mid log phase, induced for protein expression using IPTG, cold shocked by letting the cells grow at 10 °C for 24 h, and then returned to normal growth at 37 °C.

Figure 10 displays the observed growth patterns and demonstrates that *E. coli* cells transfected with the pET46-FL-HvGR-RBP1 vector grow more rapidly than cells harboring a control pET46-IsdB[N1] vector, following return to normal growth at 37 °C. Similar results are observed for *E. coli* cells harboring the pET46-N-HvGR-RBP1 vector, which leads to increased expression of the protein N-terminal RRM domain. In contrast, *E. coli* cells containing the pET32-C-HvGR-RBP1 vector encoding only the C-terminal glycine-rich region of the protein grew at a slower rate, similar to *E. coli* cells containing the control vector pET46-IsdB[N1]. Interestingly, cells transformed with the pET-FL-HvGR-RBP1(F54A), in which Phe 54 is replaced by Ala in the full-length protein and corresponding to a mutation within the consensus RNP1 RNA-binding site of
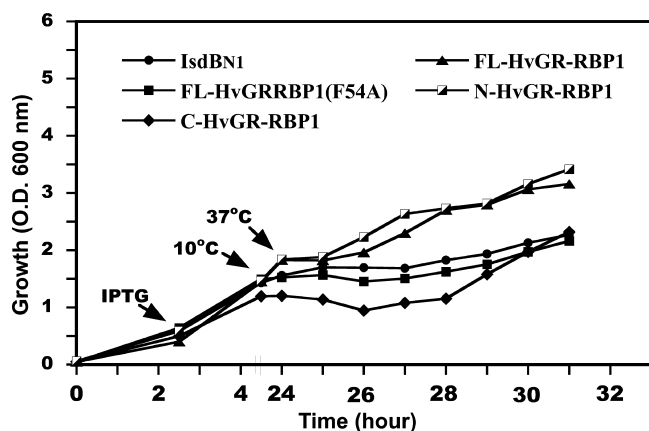
Figure 10. Growth curves of *E. coli* cells expressing FL-*Hv*GR-RBP1 (i.e., full-length protein), N-*Hv*GR-RBP1 (N-terminal RRM domain), C-*Hv*GR-RBP1 (C-terminal glycine-rich domain), FL-*Hv*GR-RBP1-(F54A) (a full-length *Hv*GR-RBP1 variant with a Phe to Ala amino acid substitution at residue position 54, which is located within the RNP1 consensus sequence of the RRM domain of *Hv*GR-RBP1), and IsdBN1 (a control protein expressed in the same pET46 plasmid as the ones encoding the different *Hv*GR-RBP1 protein constructs), following cold shock growth conditions (10 °C for 24 h) followed by a return to normal growth conditions at 37 °C.

RRMs,[22] lose their ability to grow well following cold shock treatment (Figure 10).

Taken together, these results demonstrate that the N-terminal RRM domain of *Hv*GR-RBP1 is necessary for enhanced *E. coli* growth following cold shock treatment, while the C-terminal glycine-rich domain of *Hv*GR-RBP1 does not appear to play a significant role in this cold adaptation function. Furthermore, and analogous to findings about *At*GRP7 and other *Arabidopsis thaliana* GRPs,[47−50] these results suggest that *Hv*GR-RBP1 may possess RNA chaperone activity, a function that has been associated with other plant RRM-containing glycine-rich RNA-binding proteins, in addition to other potential post-transcriptional regulatory functions such as alternative splicing, which has been established in its closest *Arabidopsis* ortholog *At*GRP7.[64,65]

■ DISCUSSION

In this manuscript, we report the detailed structural characterization and nucleic acid binding properties of the barley *Hv*GR-RBP1 protein whose transcript has been identified as being >40-fold up-regulated in early senescing "10_11" barley plants. We have shown that the N-terminal domain of *Hv*GR-RBP1 adopts a $\beta1$-$\alpha1$-$\beta2$-$\beta3$-$\alpha2$-$\beta4$ structural topology which is characteristic of canonical RNA Recognition Motifs (RRMs). The structural fold of N-*Hv*GR-RBP1 is further augmented by the presence of two β-hairpin structures that form within loops 3 and 5 and span the $\beta2$-$\beta3$ and $\alpha2$-$\beta4$ structural elements of the protein, respectively. While the two hairpins are not typically present in the loop regions of other RRMs, a single β-hairpin bridging $\alpha2$ and $\beta4$ is often observed and is involved in RNA binding, with amino acid side chains of residues within the hairpin participating in H-bonding to bases of nucleic acid targets.[66−68]

The RRM motif is found ubiquitously in all kingdoms of life and is one of the most common protein folds found in eukaryotes. Functionally, RRM-containing proteins participate in all post-transcriptional aspects of gene expression, e.g., RNA

splicing, transcript stability and degradation, RNA transport, capping, translation, termination, and RNA chaperone activity.[22,69] Further, RNA-binding proteins with one or more RRMs can be adapted to incorporate a variety of auxiliary motifs such as Arg/Asp-repeats, Ser/Arg-repeats, Arg-rich motifs, zinc finger motifs, and Gly-Tyr-Arg rich motifs as observed in *Hv*GR-RBP1.[13,17]

Interestingly, RNA-binding proteins comprising an N-terminal RRM domain and a C-terminal glycine-rich region are found ubiquitously but preferentially in plant species, which possibly highlights a specific functional role of the glycine-rich C-terminal domain, separate from the RRM domain function.

Analysis of the RRM fold of *Hv*GR-RBP1 shows that it possesses a high degree of structural similarity to the recently solved RRM domain of the *Nicotiana tabacum Nt*GR-RBP1 protein, which, combined with the high sequence identity of *Hv*GR-RBP1 to *Arabidopsis thaliana At*GRP7, suggests that these proteins share similar functional properties.

NMR investigations of the glycine rich region of *Hv*GR-RBP1 indicate that it is unstructured. A recent study of *Nicotiana tabacum Nt*GR-RBP1 showed that despite the disorder, the glycine-rich region of *Nt*GR-RBP1 can interact in trans with the RRM domain of another *Nt*GR-RBP1, indicating the potential for self-association.[24] A similar effect is observed with barley *Hv*GR-RBP1. Full-length *Hv*GR-RBP1 was found to be prone to aggregation and/or intermolecular association at high concentrations resulting in broadened NMR signals and line-shapes. Moreover, we found that the $^1H/^{15}N$ amide resonances corresponding to the RRM domain of *Hv*GR-RBP1 could be clearly distinguished from random coil signals corresponding to *Hv*GR and that the former experience small but significant chemical shift changes in the presence of *Hv*GR, suggesting that the two domains of the protein can interact. Interactions between *Hv*GR and RRM could be, however, abrogated by varying the temperature or pH conditions of the samples. These results suggest that the interactions between *Hv*GR and the RRM domain are weak and, most likely, very dynamic.

A truncated construct lacking the 25 most C-terminal residues of the full-length protein, 137-*Hv*GR-RBP1, also eliminated these chemical shift perturbation effects, suggesting that the very C-terminal end of *Hv*GR is required for interactions with the RRM domain of *Hv*GR-RBP1. The fact that we observed chemical shift changes for resonances of the full-length protein could indicate that the full-length protein may adopt a more compact structure in the absence of binding to nucleic acid polymers.

Despite the unstructured nature of the GR domain, nucleic acid binding to FL-*Hv*GR-RBP1 shows that this region can interact with ssRNA in EMSA experiments. However, this ssRNA binding appears to be nonspecific. A hybrid fusion protein composed of *Hv*GR and thioredoxin retained ssRNA-binding ability, while truncation of the 25 most C-terminal residues of the full-length protein is sufficient to eliminate this effect. Interestingly, we observed frequently during the course of our experiments that the glycine-rich region is quite susceptible to protease degradation, which eliminated the ability of resulting protein products to bind ssRNA in the EMSA experiments. This susceptibility for degradation could indicate a control level for *Hv*GR-RBP1 whereby the activity of the protein is rapidly turned off by protease cleavage of C-terminal residues within the GR domain of the protein.

The apparent absence of ssRNA binding to the RRM domain of N-HvGR-RBP1 in the *in vitro* EMSA assays is attributed to the specificity requirements of the RRM domain for well-defined nucleotide sequences, combined with the inherently low affinity of isolated RRMs for ssRNA targets, as has been observed for most RRMs when isolated from the rest of their protein scaffolds.[20] We did, however, find that the RRM domain of HvGR-RBP1 interacts with several nucleotide target sequences using 2D ^{1}H/^{15}N chemical shift experiments. Similarly to what was observed by Khan et al. in their studies of NtGR-RBP1,[24] titration of ssDNA 6nt oligonucleotides 5′-TTCTGA-3′ and 5′-TTCTGT-3′, which are part of the 5′-intronic region and 3′-UTR of the $Hvgr$-$rbp1$ gene, caused several ^{1}H/^{15}N chemical shift changes of N-HvGR-RBP1 amide resonances. Residues affected by the binding of the 6-nucleotide ssDNAs to N-HvGR-RBP1 corresponded to amino acid residues positioned within the RNP2 and RNP1 consensus RNA-binding sites of the RRM motif. The two oligonucleotide sequences that are naturally present in the $Hvgr$-$rbp1$ pre-mRNA transcript contain the same CTG element that was identified by Khan et al. to be a key element within the 5′-TTCTGG-3′ oligonucleotide sequence observed to bind to NtGR-RBP1.[24] In our study, we investigated the binding of a third ssDNA oligonucleotide fragment (i.e., 5′-CTGTTG-3′) to N-HvGR-RBP1, in which the CTG element was retained but the other nucleotides scrambled. Such a "scrambled" 6-nt oligonucleotide ssDNA sequence resulted in significantly weaker binding to N-HvGR-RBP1 ($\sim$550 μM K_d compared to equilibrium dissociation constants of $\sim$4−43 μM for other ssDNA ligands), indicating that the nucleotides adjacent to the CTG element are indeed important modulators of the RRM binding affinity for its ssDNA target. These data support that the nucleotide binding surface of the RRM domain of HvGR-RBP1 is at least $\sim$6−8 nt long, consistent with what has been reported for NtGR-RBP1.[24]

Overall, the binding of HvGR-RBP1 to these two specific 5′-TTCTGA-3′ and 5′-TTCTGT-3′ sequences strongly suggests that HvGR-RBP1 may also function as an alternative splicing regulator of its own pre-mRNA transcript, similar to what has been observed for the *Arabidopsis* AtGRP7 protein.[25,65] Based on these results, we propose a nucleotide-binding model for HvGR-RBP1 in which the synergistic interactions between the protein RRM and GR domains enhance the affinity of HvGR-RBP1 for its target single-stranded nucleic acid sequences.

To date, the expression profiles of several GR-RBPs have been studied under different environmental stress conditions, whereby the data clearly indicate that these proteins are involved in plant responses to various environmental factors.[48,50] In our studies, we observed that $Hvgr$-$rbp1$ transcript expression is up-regulated following cold stress treatment (Supporting Information Figure S3). Our cold stress experiments suggest that HvGR-RBP1 harbors RNA folding chaperone activity, similarly to what has been observed for AtGRP7,[48,50] although the glycine-rich domain of HvGR-RBP1 does not appear essential for this function. Our results are consistent with previous studies which have shown that only the RRM domain of GR-RBPs is necessary for RNA chaperone activity in bacteria.[70,71] Similarly, DNA melting experiments, used as a proxy for demonstrating RNA chaperone function, have shown that the single RRM domain of NtGR-RBP1 is sufficient to induce DNA melting of CTG-containing fragments.[24] Recent studies using photoelectric transfer (PET) fluorescence spectroscopy to investigate the interaction of

AtGRP7 with its ssRNA target have suggested that RRM domain binding to an extended form of its ssRNA target prevents formation of RNA hairpin structures.[25] Analogies to the mode of function of AtGRP7 and NtGR-RBP1 thus suggest that the mechanism of RNA chaperone function of HvGR-RBP1 resides in its ability to prevent the formation of undesirable RNA secondary structure. Interestingly, it has been noted that plant GR-RBPs involved in cold adaptation share sequence homology to cold-induced cyanobacteria proteins, which are composed of one or more N-terminal RRM motifs and a C-terminal glycine-rich domain.[70−72]

Lastly, it remains to be established whether HvGR-RBP1 possesses regulatory activity influencing or controlling multiple cellular functions, similar to what has been observed for *Arabidopsis* GRPs. For example, *Arabidopsis thaliana* glycine-rich RNA-binding proteins 7 and 8 (AtGRP7 and AtGRP8 which share 65% and 63% sequence identity with HvGR-RBP1) have been implicated in numerous biological processes including but not limited to circadian clock-controlled mechanisms,[65] plant pathogen defense,[73] and plant flowering control,[8] in addition to a possible role in senescence. Furthermore, Streitner et al.[8] demonstrated that *Arabidopsis thaliana* lines without AtGRP7 functionality flower somewhat later under long days, and considerably later under short days when compared to corresponding wild-type germplasm.[8] In contrast, *Arabidopsis* plants overexpressing AtGRP7 flower earlier.[8] These results parallel observations with early senescing barley line "10_11" that expresses high levels of $Hvgr$-$rbp1$ transcripts,[5,11] suggesting that HvGR-RBP1 and AtGRP7 share at least some regulatory functions in plant development. Studies aimed at identifying additional regulatory functions for HvGR-RBP1 in barley plants are currently ongoing.

In summary, we have solved the 3D solution NMR structure of barley HvGR-RBP1, which has been identified as a potential regulator of barley leaf and whole-plant senescence. We have shown that FL-HvGR-RBP1 is a two-domain protein, composed of a well-folded N-terminal RRM motif and an unstructured C-terminal GR domain. We have shown that the RRM domain of HvGR-RBP1 binds nucleotide fragments containing the consensus nucleotide sequence 5-TTCTGX-3′ with low micromolar affinity *in vitro*. We have also demonstrated that the C-terminal GR domain of Hv-GR-RBP1 can interact with ssRNA *in vitro* in a nonspecific manner. Based on protein expression analysis and *E. coli* growth studies following cold shock treatment, we conclude that HvGR-RBP1 can function in a manner similar to that of cold-shock proteins and may harbor RNA chaperone activity that confers cold-stress tolerance to barley plants.

■ ASSOCIATED CONTENT

ⓢ Supporting Information

Supplementary Figures S1−S5 and Supplementary Table S1: Figure S1 depicts a multiple sequence alignment of HvGR-RBP1 with plant, protozoan, microbial, and eukaryotic RRM-containing proteins. Figure S2 represents a structural overlay of HvGR-RBP1 with mammalian RRM domains. Figure S3 is a graphical representation of the effect of cold stress in barley on $Hvgr$-$rbp1$ transcript expression. Figure S4 represents an overlay of the 2D ^{1}H−^{15}N HSQC spectra of FL-HvGR-RBP1 (in black) and N-HvGR-RBP1 (in red) recorded at pH 7.2 and temperature of 303 K. Figure S5 presents the 2D ^{1}H−^{15}N HSQC spectra of the truncated constructs 137-HvGR-RBP1 (Figure S5A) and 112-HvGR-RBP1 (Figure S5B) recorded at

pH 6.8 and temperature of 298 K. Table S1 reports equilibrium dissociation constants (K_d) obtained from titration experiments whereby varying concentrations of unlabeled 6-nucleotide ssDNA ligands were added to ^{15}N-labeled N-HvGRRBP1 NMR samples followed by the recording of series of 2D [1]H−^{15}N HSQC NMR spectra, and the analysis of ^{1}H/^{15}N chemical shift changes upon ligand binding. These data support the notion that the RRM domain of HvGR-RBP1 exhibits micromolar binding affinity for 6nt ssDNA targets in these in vitro experiments. This material is available free of charge via the Internet at http://pubs.acs.org.

■ AUTHOR INFORMATION

Corresponding Author

*E-mail: vcopie@chemistry.montana.edu. Phone: (406) 994-7244. Fax: (406) 994-5407.

Notes

The authors declare no competing financial interest.

■ ACKNOWLEDGMENTS

■ ABBREVIATIONS

AtGRP7, Arabidopsis thaliana glycine-rich RNA-binding protein 7; AtGRP8, Arabidopsis thaliana glycine-rich RNA-binding protein 8; BMRB, BioMagResBank database; CSD, cold shock domain; dpa, days past anthesis; DSS, 4,4-dimethyl-4-silapentane-1-sulfonic acid; EDTA, ethylene-diaminetetraacetic acid; EMSA, electrophoretic mobility shift assay; GPC, grain protein content; GRP, glycine-rich proteins; HSQC, heteronuclear single quantum coherence spectroscopy; HvGR-RBP1, Hordeum vulgare L. Glycine-Rich RNA-Binding Protein 1; IPTG, isopropyl β-thiogalactoside; NMR, nuclear magnetic resonance spectroscopy; NOESY, nuclear Overhauser enhancement spectroscopy; NOE, nuclear Overhauser effect; PDB, Protein Data Bank; RMA, robust multiarray average; RMSD, root-mean-squared deviation; RRM, RNA recognition motif; ss/ds RNA/DNA, single-stranded/double-stranded RNA/DNA; SSM, secondary structure matching; TBE buffer, Tris/Borate/EDTA buffer

■ REFERENCES

(1) Zhang, H., and Zhou, C. (2013) Signal transduction in leaf senescence. Plant Mol. Biol. 82, 539−545.

(2) Distelfeld, A., Avni, R., and Fischer, A. M. (2014) Senescence, nutrient remobilization, and yield in wheat and barley. J. Exp. Bot. 65, 3783−3798.

(3) See, D., Kanazin, V., Kephart, K., and Black, T. (2002) Mapping genes controlling variation in barley grain protein concentration. Crop Sci. 42, 680−685.

(4) Gregersen, P. L. (2011) Senescence and nutrient remobilization in crop plants, In The molecular and physiological basis of nutrient use efficiency in crops (Hawkesford, M. J., and Barraclough, P. B., Eds.), pp 83−102, John Wiley & Sons, Oxford, UK.

(5) Jukanti, A., Heidlebaugh, N., Parrott, D., Fischer, I., McInnerney, K., and Fischer, A. (2008) Comparative transcriptome profiling of near-isogenic barley (Hordeum vulgare) lines differing in the allelic state of a major grain protein content locus identifies genes with possible roles in leaf senescence and nitrogen reallocation. New Phytologist 177, 333−349.

(6) Jukanti, A. K., and Fischer, A. M. (2008) A high-grain protein content locus on barley (Hordeum vulgare) chromosome 6 is associated with increased flag leaf proteolysis and nitrogen remobilization. Physiol. Plant. 132, 426−439.

(7) Heidlebaugh, N. M., Trethewey, B. R., Jukanti, A. K., Parrott, D. L., Martin, J. M., and Fischer, A. M. (2008) Effects of a barley (Hordeum vulgare) chromosome 6 grain protein content locus on whole-plant nitrogen reallocation under two different fertilization regimes. Funct. Plant Biol. 35, 619−632.

(8) Streitner, C., Danisman, S., Wehrle, F., Schoning, J. C., Alfano, J. R., and Staiger, D. (2008) The small glycine-rich RNA binding protein AtGRP7 promotes floral transition in Arabidopsis thaliana. Plant J. 56, 239−250.

(9) Gepstein, S., Sabehi, G., Carp, M.-J., Hajouj, T., Nesher, M. F. O., Yariv, I., Dor, C., and Bassani, M. (2003) Large-scale identification of leaf senescence-associated genes. Plant J. 36, 629−642.

(10) Lacerenza, J. A., Parrott, D. L., and Fischer, A. M. (2010) A major grain protein content locus on barley (Hordeum vulgare L.) chromosome 6 influences flowering time and sequential leaf senescence. J. Exp. Bot. 61, 3137−3149.

(11) Parrott, D. L., Downs, E. P., and Fischer, A. M. (2012) Control of barley (Hordeum vulgare L.) development and senescence by the interaction between a chromosome six grain protein content locus, day length, and vernalization. J. Exp. Bot. 63, 1329−1339.

(12) Lorkovic, Z. J. (2009) Role of plant RNA binding proteins in development, stress response, and genome organization. Trends Plant Sci. 14, 229−236.

(13) Mangeon, A., Junqueira, R. M., and Sachetto-Martins, G. (2010) Functional diversity of the plant glycine-rich proteins superfamily. Plant Sign. Behav. 5, 99−104.

(14) Sachetto-Martins, G., Franco, L. O., and de Oliveira, D. E. (2000) Plant glycine-rich proteins: a family or just proteins with a common motif? Biochim. Biophys. Acta 1492, 1−14.

(15) Alba, M. M., and Pages, M. (1998) Plant proteins containing the RNA recognition motif. Trends Plant Sci. 3, 15−21.

(16) Lorkovic, Z. J., and Barta, A. (2002) Genome analysis: RNA recognition motif (RRM) and K homology (KH) domain RNA-binding proteins from the flowering plant Arabidopsis thaliana. Nucleic Acids Res. 30, 623−635.

(17) Ambrosone, A., Costa, A., Leone, A., and Grillo, S. (2012) Beyond transcription: RNA binding proteins as emerging regulators of plant response to environmental constraints. Plant Sci. 182, 12−18.

(18) Kang, H., Park, S. J., and Kwak, K. J. (2013) Plant RNA chaperones in stress response. Trends Plant Sci. 18, 100−106.

(19) Woloshen, V., Huang, S., and Li, X. (2011) RNA-binding proteins in plant immunity. J. Pathogens 2011, 278697.

(20) Clery, A., Blatter, M., and Allain, F. (2008) RNA recognition motifs: boring? Not quite. Curr. Opin. Struct. Biol. 18, 290−298.

(21) Daubner, G. M., and Allain, F. H. (2013) RRM-RNA recognition: NMR or crystallography···and new findings. Curr. Opin. Struct. Biol. 23, 100−108.

(22) Maris, C., Dominguez, C., and Allain, F. (2005) The RNA recognition motif, a plastic RNA-binding platform to regulate post-transcriptional gene expression. *FEBS Lett. 272*, 2118−2131.

(23) Sforca, M. L., Domingues, M. N., Zeri, A. C. M., and Benedetti, C. E. (2014) Structural determination of the *Citrus sinensis* Poly(A)-Binding Protein CsPABP1. *PDB ID 2M70*; No associated publication to date.

(24) Khan, F., Daniels, M. A., Folkers, G. E., Boelens, R., Naqci, S. M. S., and van Ingen, H. (2014) Structural basis of nucleic acid binding by *Nicotania tabacum* glycine-rich RNA binding protein: implications for its RNA chaperone function. *Nucleic Acids Res. 42*, 8705−8718.

(25) Schuttpelz, M., Schoning, J. C., Doose, S., Neuwiler, H., Peters, E., Staiger, D., and Sauer, M. (2008) Changes in conformational dynamics of mRNA upon *At*GRP7 binding studied by fluorescence correlation spectroscopy. *J. Am. Chem. Soc. 130*, 9507−9513.

(26) Mason, K. E., Tripet, B. P., Parrott, D., Fischer, A. M., and Copié, V. (2014) 1H, 13C, 15N backbone and side chain NMR resonance assignments for the N-terminal RNA recognition motif of the HvGR-RBP1 protein involved in the regulation of barley (*Hordeum vulgare* L.) senescence. *Biomol. NMR Assign. 8*, 149−153.

(27) Delaglio, F., Grzesiek, S., Vuister, G. W., Zhu, G., Pfeifer, J., and Bax, A. (1995) NMRPipe- a multidimensional spectral processing system based on unix pipes. *J. Biomol. NMR 6*, 277−293.

(28) Goddard, T. D., and Kneller, D. G.. (2008) *SPARKY 3*, University of California, San Francisco.

(29) Shen, Y., Delaglio, F., Cornilescu, G., and A, B. (2009) TALOS+: a hybrid method for predicting protein backbone torsion angles from NMR chemical shifts. *J. Biomol. NMR. 44*, 213−223.

(30) Willard, L., Ranjan, A., Zhang, H., Monzavi, H., Boyko, R., Sykes, B., and Wishart, D. S. (2003) VADAR: a web server for quantitative evaluation of protein structure quality. *Nucleic Acids Res. 31*, 3316−3319.

(31) Hwang, T., van Zill, P., and Mori, S. (1998) Accurate Quantitation of Water-amide Proton Exchange Rates Using the Phase-Modulated CLEAN Chemical EXchange (CLEANEX-PM) Approach with a Fast-HSQC (FHSQC) Detection Scheme. *J. Biomol. NMR 11*, 221−226.

(32) Guntert, P. (2004) Automated NMR structure calculation with CYANA. *Methods Mol. Biol. 278*, 353−378.

(33) Guntert, P., Mumenthaler, C., and Wuthrich, K. (1997) Tosion angle dynamics for NMR structure calculation with the new program DYANA. *J. Mol. Biol. 273*, 283−298.

(34) Case, D. A., Darden, T. A., Cheatham, I, T, E., Simmerling, C. L., Wang, J., Duke, R. E., Luo, R., Merz, K. M., Pearlman, D. A., Crowley, M., Walker, R. C., Zhang, W., Wang, B., Hayik, S., Roitberg, A., Seabra, G., Wong, K. F., Paesani, F., Wu, X., Brozell, S., Tsui, V., Gohlke, H., Yang, L., Tan, C., Mongan, J., Hornak, V., Cui, G., Beroza, P., Mathews, D. H., Schafmeister, C., Ross, W. S., and Kollman, P. A. (2006) *AMBER 9*, University of California, San Francisco.

(35) Bertini, I., Case, D. A., Ferella, L., Giachetti, A., and Rosato, A. (2011) A Grid-enabled web portal for NMR structure refinement with AMBER. *Bioinformatics 27*, 2384−2390.

(36) Laskowski, R. A., Rullmann, J. A. C., MacArthur, M. W., Kaptein, R., and Thornton, J. M. (1996) AQUA and PROCHECK-NMR: Programs for checking the quality of protein structures solved by NMR. *J. Biomol. NMR 8*, 477−486.

(37) Chen, V. B., Arendall, W. B., Headd, J. J., Keedy, D. A., Immormino, R. M., Kapral, G. J., Murray, L. W., Richardson, J. S., and Richardson, D. C. (2010) MolProbity: all-atom structure validation for macromolecular crystallography. *Acta Crystallogr., Sect. D 66*, 12−21.

(38) Luthy, R., Bowie, J. U., and Eisenberg, D. (1992) Assessment of protein models with 3-dimensional profiles. *Nature 356*, 83−85.

(39) Bhattacharya, A., Tejreo, R., and Montelione, G. T. (2007) Evaluating protein structures determined by structural genomics consortia. *Proteins 66*, 778−795.

(40) DeLano, W. L. (2002) *The PyMol. Molecular Graphics System*; DeLano Scientific, San Carlos, CA.

(41) Holm, L., and Rosenstrom, P. (2012) Dali server: conservation mapping in 3D. *Nucleic Acids Res. 38*, W545−W549.

(42) Holm, L., Kaariainen, S., Rosenstrom, P., and Schenkel, A. (2008) Searching protein structure databases with DaliLite v.3. *Bioinformatics 24*, 2780−2781.

(43) Johnson, M., Zaretskaya, I., Raytselis, Y., Merezhuk, Y., McGinnis, S., and Madden, T. L. (2008) NCBI BLAST: a better web interface. *Nucleic Acids Res. 36*, W5−W9.

(44) Siever, F., Wilm, A., Dineen, D. G., Gibson, T. J., Karplus, K., Li, W., Lopez, R., McWilliam, H., Remmert, M., Söding, J., Thompson, J. D., and Higgins, D. G. (2011) Fast, scalable generation of high-quality protein multiple sequence alignments using Clustal Omega. *Mol. Syst. Biol. 7*, 539.

(45) Smith, C. W. J. (2002) *RNA:Protein Interactions: A practical approach*, Oxford University Press, Oxford, UK.

(46) Bodenhausen, G., and Ruben, D. J. (1980) Natural abundance nitrogen-15 NMR by enhanced heteronuclear spectroscopy. *Chem. Phys. Lett. 69*, 185−189.

(47) Kim, J. Y., Kim, J. S., and Kang, H. (2005) Cold-inducible zinc finger-containing glycine-rich RNA binding protein contributes to the enhancement of freezing tolerance in *Arabidopsis thaliana*. *Plant J. 42*, 890−900.

(48) Kim, J. Y., Park, S. J., Kwak, K. J., Kim, J. O., Kim, J. Y., Song, J., Jang, B., Jung, C.-H., and Kang, H. (2007) Cold shock domain proteins and glycine-rich RNA-binding proteins from *Arabidopsis thaliana* can promote the cold adaptation process in *Escherichia coli*. *Nucleic Acids Res. 35*, 506−516.

(49) Kim, J. Y., Kim, W. Y., Kwak, K. J., Oh, S. H., Han, Y. S., and Kang, H. (2010) Glycine-rich RNA-binding proteins are functionally conserved in *Arabidopsis thaliana* and *Oryza sativa* during cold adaptation process. *J. Exp. Bot. 6*, 2317−2325.

(50) Kwak, K. J., Park, S. J., Han, J. H., Kim, M. K., Oh, S. H., Han, Y. S., and Kang, H. (2011) Structural determinants crucial to the RNA chaperone activity of glycine-rich RNA-binding proteins 4 and 7 in *Arabidopsis thaliana* during the cold adaptation process. *J. Exp. Bot. 62*, 4003−4011.

(51) Dash, S., Van Hemert, J., Hong, L., Wise, R. P., and Dickerson, J. A. (2012) PLEXdb: gene expression resources for plants and plant pathogens. *Nucleic Acids Res. 40*, D1194−D1201.

(52) Close, T. J., Wanamaker, S. I., Caldo, R. A., Turner, S. M., Ashlock, D. A., Dickerson, J. A., Wing, R. A., Muehlbauer, G. J., Kleinhofs, A., and Wise, R. P. (2004) A new resource for cereal genomics: 22K barley GeneChip comes of age. *Plant Phys. 134*, 960−968.

(53) Irizarry, R. A., Hobbs, B., Collin, F., Beazer-Barclay, Y., Antonellis, K. J., Scherf, U., and Speed, T. P. (2003) Exploration, normalization, and summaries of high density oligonucleotide array probe level data. *Biostatistics 4*, 249−264.

(54) Heintzen, C., Nater, M., Apel, K., and Staiger, D. (1997) *At*GRP7, a nuclear RNA-binding protein as a component of a circadian-regulated negative feedback loop in *Arabidopsis thaliana*. *Proc. Natl. Acad. Sci. U.S.A. 94*, 8515−8520.

(55) Carpenter, C. D., Kreps, J. A., and Simon, A. E. (1994) Genes encoding glycine-rich *Arabidopsis thaliana* proteins with RNA-binding motifs are influenced by cold treatment and an endogenous circadian rhythm. *Plant Phys. 104*, 1015−1025.

(56) Messais, A. C., and Sattler, M. (2004) Structural basis of single-stranded RNA recognition. *Acc. Chem. Res. 37*, 279−287.

(57) Katahira, M., Miyanoiri, Y., Enokizono, Y., Matsuda, G., Nagata, T., Ishikawa, F., and Uesugi, S. (2001) Structure of the C-terminal RNA-binding domain of hnRNP D0 (AUF1), its interactions with RNA and DNA, and change in backbone dynamics upon complex formation with DNA. *J. Mol. Biol. 311*, 973−988.

(58) Krissinel, E., and Henick, K. (2004) Secondary-structure matching (SSM), a new tool for fast protein structure alignment in three dimensions. *Biol. Cryst. 60*, 2256−2268.

(59) Kumar, A. O., Swenson, M. C., Benning, M. M., and Kielkopf, C. L. (2008) Structure of the central RNA recognition motif of human TIA-1 at 1.95A resolution. *Biochem. Biophys. Res. Commun. 367*, 813−819.

(60) Safaee, N., Kozlov, G., Noronha, A. M., Xie, J., Wilds, C. J., and Gehring, K. B. (2012) Interdomain allostery promotes assembly of the polyA mRNA complex with PABP and eIF4G. *Mol. Cell 48*, 375−386.

(61) Michel, Y. M., Poncet, D., Piron, M., Kean, K. M., and Borman, A. M. (2000) Cap-poly(A) synergy in mammalian cell free extracts. Investigation of the requirements for poly(A) mediated stimulation of translation initiation. *J. Biol. Chem. 275*, 32268−32276.

(62) Melamed, D., Young, D. L., Gamble, C. E., Miller, C. R., and Fields, S. (2013) Deep mutational scanning of an RRM domain of the Saccharomyces cerevisiae poly(A) binding protein. *RNA 19*, 1537−1551.

(63) Staiger, D., Zecca, L., Wieczorek, K. D. A., Apel, K., and Eckstein, L. (2003) The circadian clock regulated RNA-binding protein AtGRP7 autoregulates its expression by influencing alternative splicing of its own pre-mRNA. *Plant J. 33*, 361−371.

(64) Streitner, C., Koster, T., Simpson, C. G., Shaw, P., Danisman, S., Brown, J. W. S., and Staiger, D. (2012) An hnRNP-like RNA binding protein affects alternative splicing by *in vivo* interaction with transcripts in *Arabidopsis thaliana. Nucleic Acids Res. 40*, 11240−11255.

(65) Schoning, J., Streitner, C., Page, D., Hennig, S., Uchida, K., Wolf, E., Furuya, M., and Staiger, D. (2007) Auto-regulation of the circadian slave oscillator component AtGRP7 and regulation of its targets is impaired by a single RNA recognition motif point mutation. *Plant J. 52*, 1119−1130.

(66) Volpon, L., D'Orsa, I., Young, C., Frasch, A., and Gehring, K. (2005) NMR structural study of TcUBP1, a single RRM domain protein from *Trypanosoma cruzi*: contribution of a beta hairpin to RNA binding. *Biochemistry 44*, 3708−3717.

(67) Auweter, S., Fasan, R., Reymond, L., Underwood, J., Black, D., Pitsch, S., and Allain, F. (2006) Molecular basis of RNA recognition by the human alternative splicing factor Fox-1. *EMBO J. 25*, 163−173.

(68) Perez-Canadillas, J., and Varani, G. (2001) Recent advances in RNA−protein recognition. *Curr. Opin. Struct. Biol. 11*, 53−58.

(69) Fedoroff, N. V. (2002) RNA-binding proteins in plants: the tip of an iceberg? *Curr. Opin. Plant Biol. 5*, 452−459.

(70) Graumann, P. L., and Marahiel, M. A. (1998) A superfamily of proteins that contain the cold shock domain. *Trends Biochem. Sci. 23*, 286−290.

(71) Maruyama, K., Sato, N., and Ohta, N. (1999) Conservation of structure and cold-regulation of RNA-binding proteins in cyanobacteria: probable convergent evolution with eukaryotic glycine-rich RNA-binding proteins. *Nucleic Acids Res. 27*, 2029−2036.

(72) Nakaminami, K., Karlson, D. T., and Imai, R. (2006) Functional conservation of cold shock domain in bacteria and higher plants. *Proc. Natl. Acad. Sci. U. S. A. 103*, 10122−10127.

(73) Fu, Z., Guo, M., Jeong, B., Tian, F., Elthon, T., Cerny, R., Staiger, D., and A, A. (2007) A type III effector ADP-ribosylates RNA-binding proteins and quells plant immunity. *Nature 446*, 284−289.